ABS Control on Modern Vehicle Equipped with Regenerative Braking

W.Li

Master of Science Thesis

Delft University of Technology

Delft Center for Systems and Control

ABS Control on Modern Vehicle Equipped with Regenerative Braking

Master of Science Thesis

For the degree of Master of Science in Systems and Control at Delft University of Technology

W.Li

November 16, 2010

Faculty of Mechanical, Maritime and Materials Engineering (3mE) · Delft University of Technology

Delft University of Technology
Department of
Delft Center for Systems and Control (dcsc)

The undersigned hereby certify that they have read and recommend to the Faculty of Mechanical, Maritime and Materials Engineering (3mE) for acceptance a thesis entitled

ABS Control on Modern Vehicle Equipped with Regenerative Braking

by

W.Li

in partial fulfillment of the requirements for the degree of

Master of Science Systems and Control

Dated: November 16, 2010

Supervisor(s):

Prof.dr.ir. E.G.M.Holweg Supervisor

Dr.ir. M.Corno Second Super

Ir. M.Gerard Third Super

Reader(s):

Ir.Edwin de Vries First Reader

Abstract

Anti-lock brake system (ABS) prevents the wheels from locking up and reduce the total braking distance as far as possible. Simply ABS systems got better over time, the current implementation is based on a traditional hydraulic disk brake and a small wheel inertia.

Seen the need for making vehicles cleaner in the future, it can be expected that an increasing amount of vehicles will be equipped with electric motors able to regenerate energy during braking. The addition of this electric motor changes the properties of the brake actuation and has an influence on the wheel inertia.

The objective of this thesis work is to study the change of dynamics induced by the regenerative braking, assess the performance of traditional ABS systems on the new vehicles and propose improvements to the ABS algorithms to suit the new requirements.

This thesis project used the software MATLAB to establish simulation model, which include the single wheel dynamic model, hydraulic brake system model, electric motor brake system model and traditional ABS controller. Finally, an integrated control scheme for regenerative braking based on anti-lock brake system is implemented. Specifically, the regenerative braking system is incorporated into ABS, the electric motor takes part in anti lock brake control. By using a low pass filtering, we built a frequency splitter controller to distribute these two brake torques and research the relationship between our two cost functions which are braking distance and recovered energy.

Test results show that the control scheme not only realizes the harmony and compatibility between electric motor brake and conventional friction brake, recovering the energy, but also fully takes the advantage of quick response of motor braking, better realizing the anti-lock braking control of vehicles. According to the test performance, we must make a trade off between the braking distance and recovered energy.

Table of Contents

List of Figures

List of Tables

Acknowledgements

I would like to thank my supervisors Prof.dr.ir.E.G.M.Holweg, Dr.ir.M.Corno and Ir.M.Gerard for their assistance during the writing of this thesis and keep track of my goal during the meetings. I would like to give a special thanks to Matteo for being of constant assistance regarding theoretical analysis during this one year thesis work, he could always figured out the place where was wrong whenever I had problems, he helped me a lot, not only with the general thesis problems, but also with the concerning of my life.

Furthermore, I will appreciate my classmates and all my friends, some new idea was generated when discussing with them, which benefited as well. Also, with them I had a very active social life in the past two years and a half in Netherlands.

At last, I want to appreciate all the professors who taught me the basic system and control theory which appeared to be highly necessary for working on this thesis project.

Delft, University of Technology W.Li
November 16, 2010

"There is no future for the automotive industry without the promotion of environmental technology. It is convinced that only companies that succeed in this area will be acceptable to society."

— *Fujio Cho*

Chapter 1

Introduction

As associated with energy independence and environmental issue, alternative fuel vehicle, especially Electric and Hybrid electric vehicles (HEV) have become part of the government policy all over the world. The United State mandated a strict fuel economy standard. China issued a new energy vehicle policy to accelerate and subsidize the deployment of electric and set a goal of 500k for 2011 [1].

Over the last decade, the benefits and limitations of hybrid vehicle ownership have become much better understood, which has led to the rapid broadening of the market. However, the economic meltdown of recent years has hurt the global auto industry, and the consumer hybrid sector has fared no better. Nevertheless, several factors will help drive the consumer hybrid vehicle market in the coming years. These factors include the anticipated post-recession rise in fuel prices, continuing advances in hybrid power trains and battery technology. ABI Research foresees the market for consumer hybrids driving ahead during the forecast period, to surpass 1.9 million units by the time 2013 rolls around (Figure 1-1)[2]. Figure 1-1 indicates an upward trend of market share of HEV sales.

A hybrid electric vehicle combines a conventional internal combustion engine (ICE) propulsion system with an electric propulsion system. Modern HEVs make use of efficiency improving technologies such as regenerative braking. When we slow the vehicle, the kinetic energy that was propelling the vehicle forward has to go somewhere. Most of it simply dissipates as heat and becomes useless. That energy, which could have been used to do work, is essentially wasted. Automotive engineers have given this problem a lot of thought and have come up with a kind of braking system that can recapture much of the car's kinetic energy and convert it into electricity, so that it can be used to recharge the car's batteries. This system is called regenerative braking.

The energy efficiency of a conventional car is only about 20 percent, with the remaining 80 percent of its energy being converted to heat through friction.The main attraction of regenerative braking is that it may be able to capture as much as half of wasted energy during braking and put it back to work. This could reduce fuel consumption by 10 to

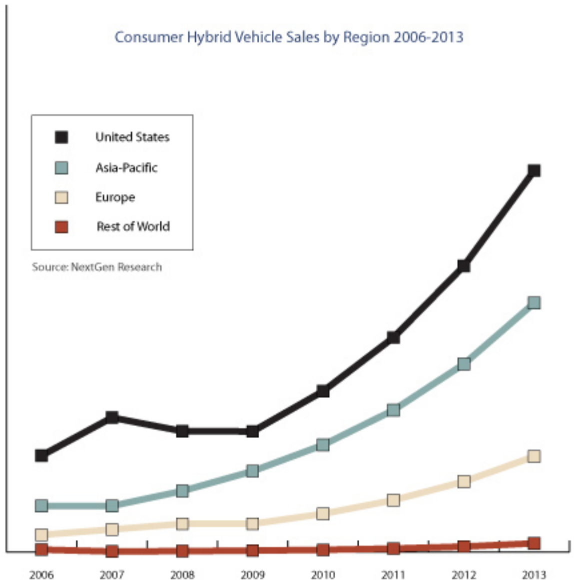

Figure 1-1: HEV market share

25 percent. Hydraulic regenerative braking systems could provide even more impressive gains, because the system promises 25-45 percent improvements in fuel economy and emissions [3]. The added efficiency of regenerative braking also means less pain at the pump, since hybrids with electric motors and regenerative brakes can travel considerably farther on a gallon of gas, some achieving more than 50 miles per gallon at this point. And that's something that most drivers can really appreciate [3].

However, in March this year (2010) Toyota company announced the recall in the whole world. Dozens of Prius drivers in Japan and the United States have complained of a short delay in braking taking effect during cold weather or on bumpy roads. More than 400,000 Prius cars and other hybrids were recalled worldwide. Concerns over safety have done deep damage to Toyota's reputation for quality and reliability which have helped it to become the largest car maker in the world. It proves the need of more research on the software configuration of regenerative braking and friction braking. Unfortunately, it is still very difficult to find in the literature a detailed description of the Anti-lock Braking System (ABS) control equipped with regenerative braking used in practice[4][5][6].

1-1 Goal and problem formulation of this thesis

The objective of this thesis is to study the change of dynamics induced by the regenerative braking, assess the performance of traditional ABS on the new vehicles and propose improvements to the ABS algorithms to satisfy the new requirements. So in this thesis, on the one hand we will study how to combine the regenerative braking and friction braking together, and the focus is currently on the straight line braking. On the other hand, braking performance by considering the braking distance and recovered energy will be investigated.

1-2 Layout

In Chapter 2, a top layer overview of the model blocks will first be presented, then the modeling of brake actuators, wheel dynamics and wheel speed sensors will be introduced respectively. The anti-lock braking system (ABS) and the approach based on wheel deceleration thresholds which is used in this project will be illustrated in Chapter 3. The regenerative braking system module and control algorithms will be discussed in Chapter 4. In the last chapter, there will be discussions drawn from the previous chapters, at the same time, the related problems when implementing the controller algorithms will also be introduced, some recommendations will be presented at the end of the thesis.

Chapter 2

System Modeling

This chapter will be devoted to introduce the dynamical models employed for the design in terms of brake actuators, quarter car model and sensors. Approaches of modeling simulation for each part also will be introduced separately.

In order to help understand the entire dynamic system, firstly we build a schematic program. Figure 2-1 gives a top layer overview of the model blocks. To have a better overview of the entire system, it is divided into three blocks: Actuators, Tyre and Wheel dynamics, and Sensors. The first block contains the hydraulic brake actuator, electric motor and transmission, also the brake caliper and the pump and brake fluid dynamics are included. The tyre and wheel dynamics subsystem contains the formulas relating the tyre and wheel's inertia to the torques and forces imposed on it. All the sensed signals from each block are passed through the sensor block.

Those three main block models in Figure 2-1 will be described separately in the following sections.

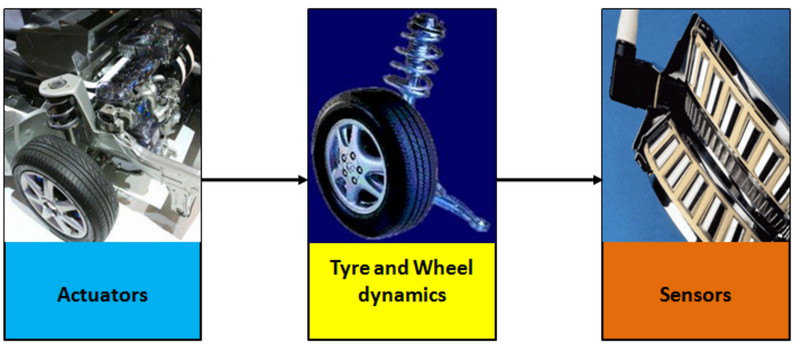

Figure 2-1: An overview of the entire system model

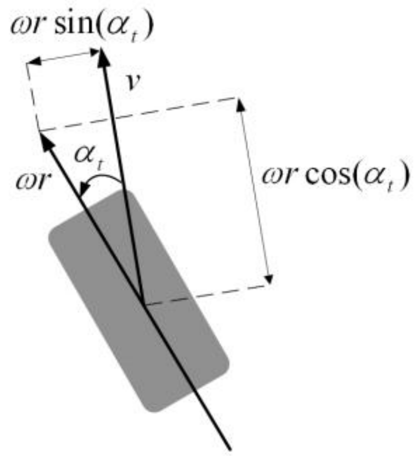

Figure 2-2: Longitudinal wheel slip

2-1 Tyre and Wheel Dynamics Modeling

2-1-1 Tyre Forces and Modeling

In general, because of tire deformation and because of traction and braking forces exerted on the tire, the wheel ground contact point velocity v is not equal to the product ωr. Denoting by the velocity of a pure rolling wheel whose radius is r and angular velocity is ω, the longitudinal slip coefficient λ can be defined as

$$\lambda = \frac{v - \omega r}{max\{v, \omega r\}} = \frac{v - \omega r \cos(\alpha_t)}{max\{v, \omega r \cos(\alpha_t)\}} \tag{2-1}$$

Where α_t is the wheel side-slip angle. In vehicle dynamics, side-slip angle is the angle between a rolling wheel's actual direction of travel and direction towards which is pointing.

Actually, we mostly concentrate on braking maneuvers taking place on a straight-line. So the equations becomes:

$$\lambda = \frac{v - \omega r}{v} \tag{2-2}$$

With $\lambda \in [0, 1]$. In particular $\lambda = 0$ corresponds to a pure rolling wheel and $\lambda = 1$ to a locked wheel.

The tractive effort coefficient and tire slip always have a relationship as shown in Figure 2-3. From this figure we can see that the tractive effort coefficient reaches the maximum value at the peak value point A. When the slip ratio is below point A, the slip ratio can increase the traction force (longitudinal curve in Figure 2-3). Once the slip ratio exceeds A, the traction force will decrease as a result of the decrease of adhesive coefficient. In addition to the tractive forces, the wheel must also generate a lateral

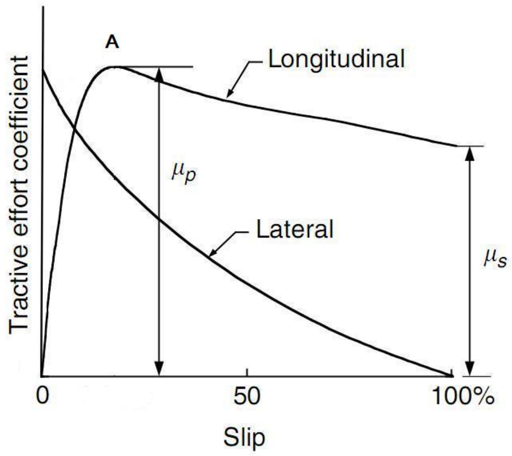

Figure 2-3: Slip-Tractive coefficient curve

force (lateral curve in Figure 2-3) to direct the vehicle. Like the tractive forces, the lateral force is also dependent on the slip ratio. The lateral force will be decreased as the slip is increased. Thus, the steering ability will be decreased as the slip is increased.

The longitudinal tyre force F_x is modeled by a relation

$$F_x(\lambda, F_z) = \mu(\lambda)F_z \tag{2-3}$$

That is, by a function that depends linearly on vertical load F_z and nonlinearly on the variable. For different road surfaces, this value is different, this can be seen from Figure 2-4, the peak value that each road condition can generate is quite different. On the asphalt dry surface, the maximum force is large, but on the snow road surface, the maximum value is really small.

The function μ is usually called the road-wheel coefficient of friction. Many empirical expressions have been developed for μ; For example, Pacejka model which is also known as the magic formula uses trigonometric functions [7]. A simplified form of Pacejka's magic formula is shown below:

$$F_x(\lambda, F_z) = Msin(L\arctan[N_k - P(B_k - \arctan(N_k))]) \tag{2-4}$$

where the analytic expression of the different terms which appear in (2-4) depend on λ, F_z and on eleven parameters $(b_0, \cdots, b_{10})$ which are related to the specific tyre properties. The three coefficients M, L and P are positive. This model is very accurate, thus it is good for simulation, but the negative is also obvious, the function is complex.

Burckhardt model [8] uses exponential functions:

$$\mu(\lambda; \theta_r) = \theta_{r1}[1 - exp(= \lambda\theta_{r2})] - \lambda\theta_{r3} \tag{2-5}$$

Note that the vector θ_r is constituted by three parameters only. The model is very simple so it is suitable for analytic purposes. By changing the values of these three

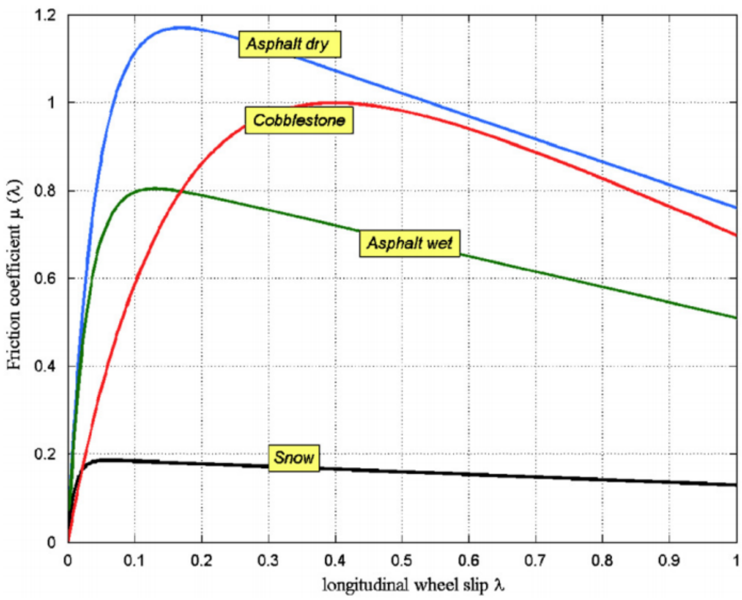

Figure 2-4: Different road surfaces map

parameters, many different road-tyre friction conditions can be modeled. In this thesis, the Burckhardt model will be employed.

2-1-2 Wheel Dynamics

In this section, we introduce a mathematical model of the wheel dynamics. The problem can be best explained by observing a quarter car model as shown in Figure 2-5. The model consists of a single wheel attached to a mass m. As the wheel rotates, driven by inertia of the mass m in the direction of the velocity v, a tyre reaction force F_x is generated by the friction between the tyre surface and the road surface. The tyre reaction force will generate a torque that initiates a rolling motion of the wheel causing an angular velocity ω. A brake torque applied to the wheel will act against the spinning of the wheel causing a negative angular acceleration. The equations of motion of the quarter car are:

$$J\dot{\omega} = rF_x - T_b \tag{2-6}$$

$$m\dot{v} = -F_x \tag{2-7}$$

- $\omega[rad/s]$ is the angular speed of the wheel;
- $v[m/s]$ is the longitudinal speed of the vehicle body;
- $T_b[Nm]$ is the braking torque;
- $F_x[N]$ is the longitudinal tyre road contact force;

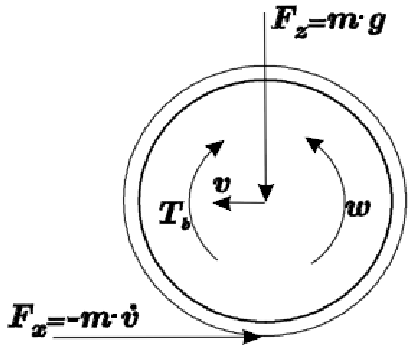

Figure 2-5: Quarter car forces and torques

- $J[kgm^2], m[kg]$ and $r[m]$ are the moment of inertia of the wheel, the quarter car mass and the wheel radius respectively.

Here an important parameter is introduced that is normalized linear wheel deceleration. It is defined as:

$$\eta = -\frac{\dot{\omega} r}{g} \tag{2-8}$$

Observer that η is the linear deceleration of the contact point of the tyre, normalized with respect to the gravitational acceleration g. It is useful since it can be easily and directly compared with the longitudinal body deceleration.

By recalling the previous expression of F_x, the following quarter car model is obtained:

$$\begin{cases} J\dot{\omega} = rF_z\mu\Big(\dfrac{v - \omega r}{v}\Big) - T_b \\ \\ m\dot{v} = -F_z\mu\Big(\dfrac{v - \omega r}{v}\Big) \end{cases} \tag{2-9}$$

In (2-9) the state variables are ω and v. Since ω, v and λ are linked by an algebraic relationship, it is possible to replace the state variable ω with the state variable λ. This can be simply obtained by plugging the following two relationships:

$$\dot{\lambda} = -\frac{r}{v}\dot{\omega} + \frac{r\omega}{v^2}\dot{v}, \omega = \frac{v}{r}(1 - \lambda)$$

into the equation (2-9), so obtaining:

$$\begin{cases} \dot{\lambda} = -\dfrac{1}{v}\Big(\dfrac{1-\lambda}{m} + \dfrac{r^2}{J}\Big)F_z\mu(\lambda) + \dfrac{r}{vJ}T_b \\ \\ m\dot{v} = -F_z\mu(\lambda) \end{cases} \tag{2-10}$$

It is assumed [9] that the longitudinal dynamics of the vehicle (expressed by the state variable v) is much slower than the rotational dynamics of the wheel (expressed by the state variable λ or ω) due to large differences in inertia. Henceforth, v is considered as a slowly-varying parameter. Under this assumption, the equation (vehicle dynamics) (2-7) is neglected, and the model reduces to a first order model of the wheel dynamics only, we work on the following system dynamics:

$$\dot{\lambda} = -\frac{1}{v}\Big(\frac{1-\lambda}{m} + \frac{r^2}{J}\Big)F_z\mu(\lambda) + \frac{r}{vJ}T_b \tag{2-11}$$

2-1-3 Analysis of Linearized Model

A possible approach for the design of a braking control system is to recast it into a standard regulation problem. So the first step is the computation and discussion of the equilibrium points for system (2-6), and linearization of the model around its equilibrium [10].

First notice that, by setting $\dot{v} = 0$ and $\dot{\omega} = 0$ in (2-6), the corresponding equilibrium is given by $\lambda = 0$ and $T_b = 0$. This corresponds to a constant speed condition without braking; apparently, this equilibrium condition is trivial and meaningless for the design of a braking controller.

By calling back our system dynamics (2-11), by replacing v as $v = \dfrac{\omega r}{1-\lambda}$, this expression can be written as

$$\dot{\lambda} = -\frac{1-\lambda}{J\omega}(\Psi(\lambda) - T_b) \tag{2-12}$$

with $\omega > 0$ and

$$\Psi(\lambda) = \Big(r + \frac{J}{rm}(1-\lambda)\Big)F_z\mu(\lambda) \tag{2-13}$$

The equilibrium points we are interested in during braking are characterized by $\dot{\lambda} = 0$.

Consider now the following variables, defined around an equilibrium point (characterized by $\bar{T}_b, \bar{\lambda}, \bar{\dot{\omega}}$ and $\bar{\eta}$):

$$\delta T_b = T_b - \bar{T}_b, \delta\lambda = \lambda - \bar{\lambda}, \delta\dot{\omega} = \dot{\omega} - \bar{\dot{\omega}}, \delta\eta = \eta - \bar{\eta}$$

Using these variables and the key definition $\mu_1(\bar{\lambda}) = \partial\mu(\lambda)/\partial\lambda \mid_{\lambda=\bar{\lambda}}$ (the slope of the $\mu(\lambda)$ curve around equilibrium), the transfer function $G_\lambda(s)$ from δT_b to $\delta\lambda$ is given by:

$$G_\lambda(s) = \frac{\dfrac{r}{vJ}}{s + \Big[\dfrac{\mu_1(\bar{\lambda})F_z}{m\bar{v}}\Big((1-\bar{\lambda}) + \dfrac{mr^2}{J}\Big)\Big]} \tag{2-14}$$

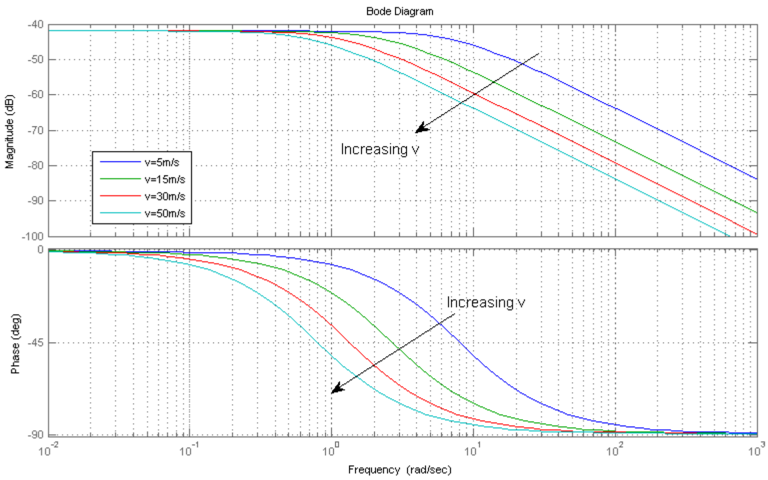

Figure 2-6: Bode plots of $G_\lambda(s)$ at different longitudinal speeds

Similarly, the transfer function $G_\eta(s)$ from δT_b to $\delta\lambda$ is given by:

$$G_\eta(s) = \frac{\frac{r}{Jg}\left[s + \left(\frac{\mu_1(\bar{\lambda})F_z}{m\bar{v}}(1-\bar{\lambda})\right)\right]}{s + \left[\frac{\mu_1(\bar{\lambda})F_z}{m\bar{v}}\left((1-\bar{\lambda}) + \frac{mr^2}{J}\right)\right]} \tag{2-15}$$

Stability condition for $G_\lambda(s)$ and $G_\eta(s)$:

$$\frac{\mu_1(\bar{\lambda})F_z}{m\bar{v}}\left((1-\bar{\lambda}) + \frac{mr^2}{J}\right) > 0$$

which can be simply reduced to $\mu_1(\bar{\lambda}) > 0$. This means that $G_\lambda(s)$ and $G_\eta(s)$ are open loop unstable if the equilibrium $\bar{\lambda}$ occurs beyond the peak of the curve $\mu(\lambda)$. Minimum-phase condition for $G_\eta(s)$:

$$\frac{\mu_1(\bar{\lambda})F_z}{m\bar{v}}(1-\bar{\lambda})$$

which can be simply reduced to $\mu_1(\bar{\lambda}) > 0$. This means that $G_\eta(s)$ is non minimum phase if the equilibrium $\bar{\lambda}$ occurs beyond the peak of the curve $\mu(\lambda)$.

Although we consider the vehicle speed v as a slow varied parameter which does not affect the stability and minimum-phase properties, it has effect on scaling the wheel dynamics. Bode plots of $G_\lambda(s)$ at different longitudinal speeds are shown in Figure 2-6.

Clearly, as the velocity is decreased, the dynamics gets faster. This scaling effect must be somehow taken into account in the design of a braking controller. This issue has been extensively considered in [11]. Assume for a moment the setpoint λ^* corresponds

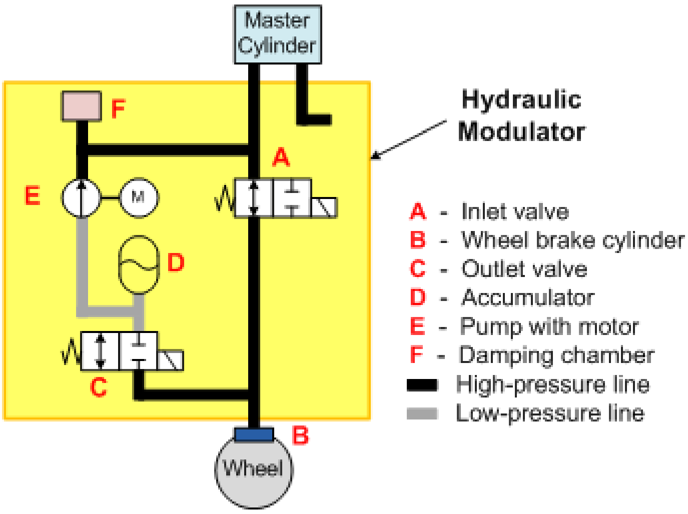

Figure 2-7: Hydraulic braking system

to a slip value near the peak of the friction cure. The family of frequency responses corresponding to values of v between 0.75 m/s and 32 m/s. It can be observed that the bandwidth (-3 dB frequency) is between 42 rad/s and 75 rad/s (depending on v). The details can be seen in [11].

2-2 Actuators Modeling

The design of automatic braking control systems is clearly highly dependent on the braking system characteristics and actuator performance. In this part, we will study the hardware of the vehicle which is important to the control system design. The currently implemented hydraulic brake actuator and the electric motor will be introduced.

2-2-1 Hydraulic Actuated Brake

Hydraulic actuated brake (HAB) uses brake fluid to apply brake pressure to pads or shoes. Most cars have a hydraulic braking system. The main parts of this system are a chamber called a master cylinder, which is located near the brake pedal; at least one wheel cylinder at each wheel; and tubes called brake pipes, which connect the master cylinder to the wheel cylinders. The cylinders and brake pipes are filled with brake fluid.

Inside the master cylinder, there is a piston, which can slide back and forth. In a simple hydraulic system, the brake pedal controls this piston by means of a rod or some other mechanical links. When the driver pushes on the pedal, the piston inside the master cylinder exerts pressure on the fluid and slides forward a short distance. The fluid transmits this pressure through the brake pipes, forcing pistons in the wheel cylinders to move forward. As the wheel cylinders move forward, they apply brake pressure to pads or shoes.

In these systems the pressure generated by the driver on the pedal is transmitted to the hydraulic system via a Inlet Valve, which communicates with the brake cylinder. Moreover, the hydraulic system has a second valve, the Outlet Valve, which can discharge the pressure and which is connected to a low pressure accumulator.

In the braking system, the braking torque acting on a wheel can be simply defined as:

$$T_b = r_d \gamma_d \cdot F_\perp \tag{2-16}$$

where T_b is braking torque, r_d is the brake disc radius, $F_\perp$ is braking force which acts on the disc vertically and γ_d is the brake pad friction coefficient. In the hydraulic brakes, this force can be expressed as

$$F_\perp = A \cdot P_b \tag{2-17}$$

where A is the brake piston area and P_b is braking pressure generated by the hydraulic fluid. Once the brake disc is fixed, the values of r_d and A are constant, so we can just use one simple equation to represent the hydraulic brake, which is:

$$T_b = \gamma \cdot P_b \tag{2-18}$$

Notice that, the parameter γ is changing during braking depending on the brake temperature. In general, the efficiency will increase with the temperature, up to a certain level where fading starts and friction drops rapidly. This means that the anti-lock braking system algorithm needs to be robust to changes in the brake properties [12].

In hydraulic braking the brake pressure P_b is our control variable, the HAB actuator is capable of providing three different control actions, namely

- Increase the brake pressure. In this case the Inlet valve is open and the Outlet one closed;
- Hold the brake pressure. In this case both valves are closed;
- Decrease the brake pressure. In this case the Inlet valve is closed and the Outlet one open.

The hydraulic dynamics model is represented in Figure 2-8. In this figure we can see, the control variable brake pressure goes through the servo-valve and the pressure flow rate can be controlled by valves, in the end it flows past the hydraulic system, and the hydraulic line a transport time delay between the desired and the actual brake pressure. These factors limit the performance of the actuation.

Some system identification work of the hydraulic dynamics model have been done in the laboratory [12], they also use a simplify model low pass filter, and the identified results of these two models almost the same, so we can simplify the dynamics into a low pass filter. A rough identification of the characteristics gives: a pure time delay

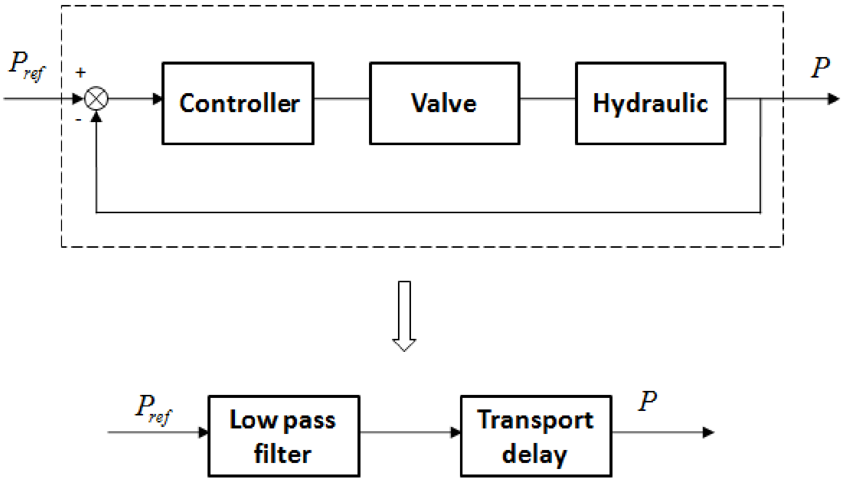

Figure 2-8: Hydraulic dynamics model

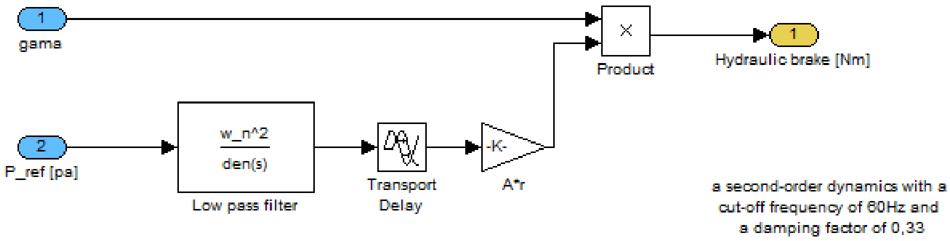

Figure 2-9: Hydraulic simulation block

$\Delta t = 7\ ms$, a pressure rate limit between $r_max = +750\ bar/s$ and $r_min = -500\ bar/s$, and a second-order dynamics with a cut-off frequency of 60 Hz and a damping factor $\xi = 0.33$. The simulation block in this design can be seen in Figure 2-9.

2-2-2 Electric Motor

An electric motor uses electrical energy to produce mechanical energy, very typically through the interaction of magnetic fields and current-carrying conductors.

In general, DC (direct current) motors are most desirable in two situations. The first is that when the only power available is DC, which occurs in automobiles and small battery powered devices. The other is when a torque-speed curve needs to be carefully doctored.

As technology and manipulation advances in AC (Alternating Current) motors, this becomes a less important aspect, but historically the DC motor has been easy to configure making it good for servo and traction application. With high current and low voltage relative to the power supplied these motors provide high torque at low speed.

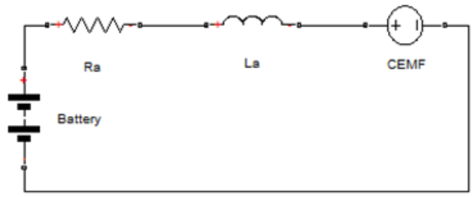

(a) Electric motor

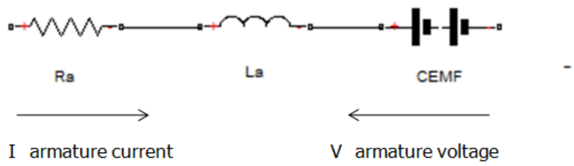

(b) Physical analysis

Figure 2-10: Equivalent circuit of a permanent motor

The variations of the standard DC motor are the universal motor, which has been slightly modified to run on AC power, and the brushless DC motor, which is a highly complex device compared with the standard motor. DC motors are used in applications requiring velocity or position control and when a high starting torque is needed as AC motors have difficulty in this area.

The control logic may change the efficiency in different motor sizes, but the control variable current is common aspect to all. An analysis of the electric motor control is coming up.

In the regeneration brake, the electric motors are most important components. Because they are reversible machines, they can function as motors or as generators.

- A motor receives electrical power from a battery and transforms it in torque developing a Counter Electromotive Force (CEMF), which opposes the battery.
- A generator receives mechanical power from a mechanical actuator and transforms it in electrical power developing a counter torque, which opposes the actuator.

Figure 2-10 represents an equivalent circuit of a permanent motor. According to the Kirchhoff's law, we can get the following equation:

$$V = E + R_a \cdot I + L_a \cdot \frac{dI}{dt} \tag{2-19}$$

where V, E, R_a, L_a, I represent armature voltage, CEMF voltage, resistance, inductance and armature current respectively.

According to the law of electromagnetic induction, we get

$$E = K_e \cdot \omega_r \tag{2-20}$$

The torque generated by a current carrying coil in magnetic field is

$$T_m = K_t \cdot I \tag{2-21}$$

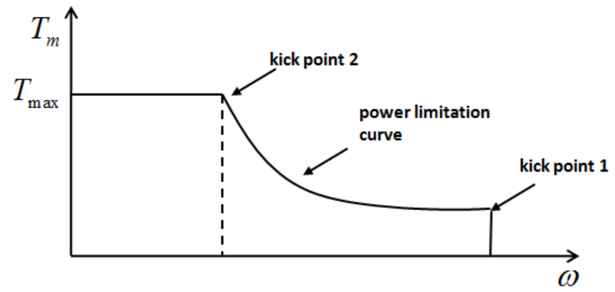

Figure 2-11: Characteristic map of the electric motor

where K_e is CEMF constant and K_t is torque constant. ω_r is rotor speed and T_m is torque motor supplied.

From equation (2-20) and (2-21), we can see that the motor torque is proportional to armature current and CEMF voltage is proportional to the speed. By controlling the current I, we can control the motor brake torque. But the limitation is that such braking force is not large enough to cover the required braking force due to the motor power limitation.

Figure 4-1 represents the characteristic curve of the electric motor. For the electric motor implementation, there are three main factors we must take into account, which are maximum torque limitation (kick point 1), maximum motor speed limitation (kick point 2) and electric motor power limitation ($P = T \cdot \omega$). In this design, the modeling of electric motor is shown in Figure 2-12.

The module named as "Limitation Compute" in Figure 2-12 is used to limit the electrical power of the system by considering the following equation:

$$P_{electric} = -RI^2 + K_e \omega I$$

we want to enforce that $P_{electric} \leq P_{max}$ (or $-P_{max}$) depending on the sign of the power flow. By solving the second order equation, the control variable current limitation I_{lim} can be found.

From the model we used in this project we can see that between the control input variable (current) and the output variable (motor torque) is a constant gain value (kt), obviously there is no limitation for the bandwidth in this model. This is the main advantage of the electric motor, no time delay. However, compare to the traditional friction brake, the maximum torque of the motor is not large.

2-2-3 Transmission

Adding the electric motor means the need of a transmission. In other words, the electric motor is connected to the opposite side of the transmission as the wheel. This vehicle configuration is shown in Figure 2-13. In this design, we use fixed gears. As with fixed

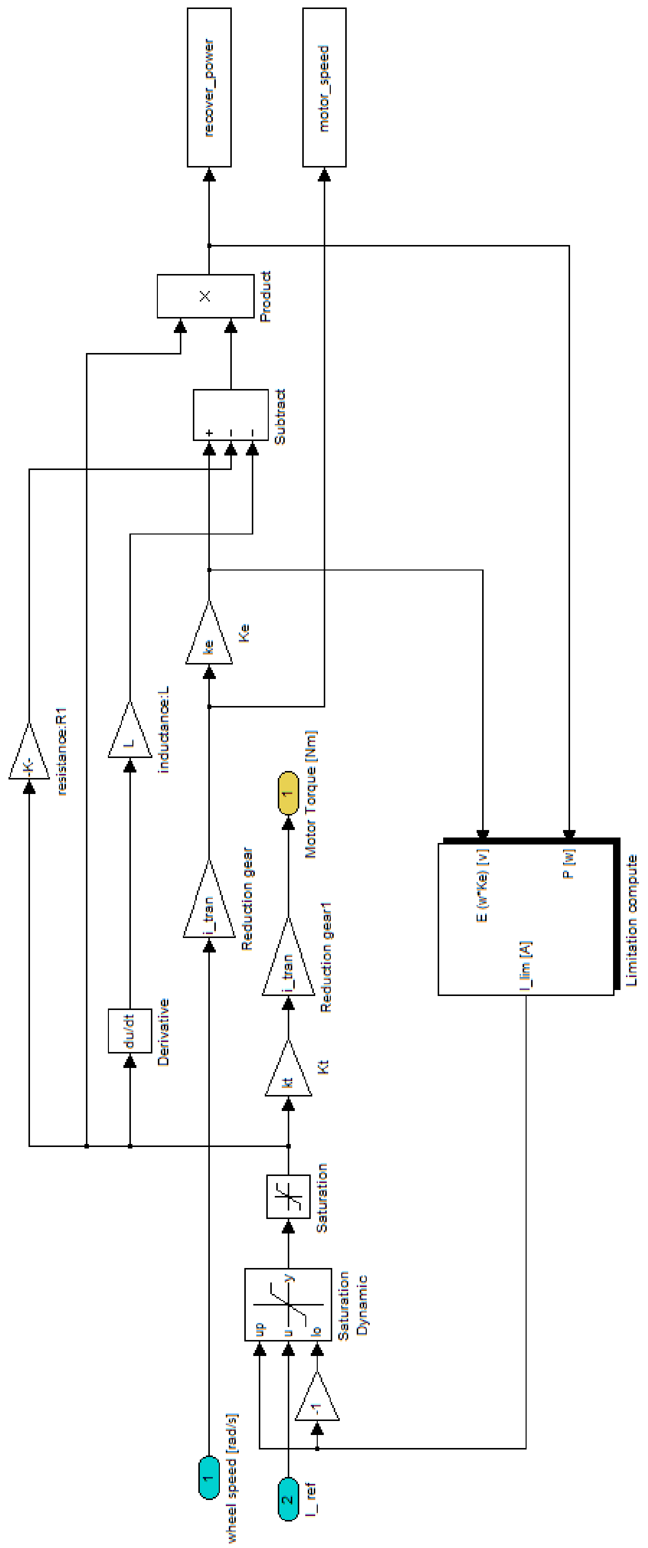

Figure 2-12: Electric motor simulation block

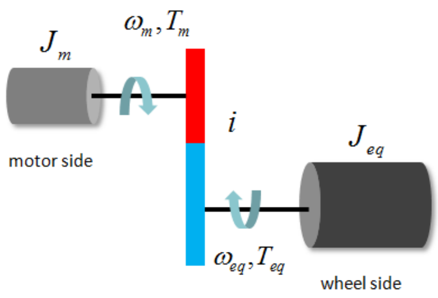

Figure 2-13: Additional inertia

gears, the transmission gear ratio is defined by the speed ratio, which is in this case the motor side speed divided by the wheel side speed.

Notice that by introducing the electric motor with the transmission, we add an extra inertia to the wheel side, so now we replace this additional inertia by an equivalent inertia on wheel side (represented by J_{eq} in Figure 2-13).

$$T_m = J_m \cdot \omega_m \tag{2-22}$$
$$T_{eq} = J_{eq} \cdot \omega_{eq} \tag{2-23}$$
$$T_{eq} = i \cdot T_m \tag{2-24}$$
$$\omega_{eq} = \frac{\omega_m}{i} \tag{2-25}$$

where J_m is motor inertia, $\omega_m, \omega_{eq}, T_m$ and T_{eq} are motor side speed, wheel side speed, motor side torque and wheel side torque respectively, i is constant transmission gear.

By doing some substitutions, we can get the equivalent inertia on wheel side:

$$J_{eq} = i^2 \cdot J_m \tag{2-26}$$

2-3 Sensors

The term sensor has become common, as in the past 20 to 40 years measuring gages have also come into use in consumer applications (e.g. motor vehicle and domestic appliance technology). Sensors-another term for measuring detectors or measuring sensors-convert a physical or chemical (generally non-electrical) variable ϕ into an electrical variable e; this process often also takes place over further, non-electrical intermediate stages.

2-3-1 Basic and Overview

The electrical sensor outputs are not only provided in the form of current and voltage, but are also available as current or voltage amplitudes, frequency, phases, pulse

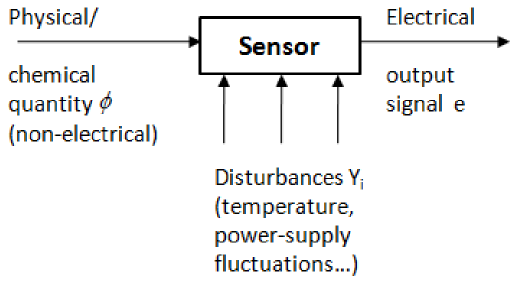

Figure 2-14: Basic sensor function

widths, and cycles or periods of an electrical oscillation, or as the electrical parameters, resistance, capacitance, and inductance. A sensor can be defined using the following equation:

1. $e = f(\Phi, Y_1, Y_2 \ldots)$ Sensor output signal
2. $\Phi = g(e, Y_1, Y_2 \ldots)$ Required measured variable

If the function f or g are known, then they represent a sensor model with the help of which the measured variables sought maybe mathematically calculated from output signal e and the influencing variables Y_i practically without error (intelligent or smart sensors)[13].

2-3-2 Wheel Speed Sensors

The ABS control algorithm implemented in this project is based on the wheel deceleration thresholds. In this control logic, the only measured variable is the wheel speed. Wheel speed sensors are used to measure it. The speed signals are transmitted via cables to the ABS control unit of the vehicle which controls the braking force individually at each wheel. This control loop prevents the wheels from locking up so that the vehicle's stability and steerability are maintained.

Since 1998 active wheel speed sensors have been used almost exclusively with new developments instead of passive (inductive) wheel speed sensors.

In the following part, we introduce the principle of this sensor. A sinusoidal signal is produced as the impulse wheel teeth opening pass in front of the sensor, which causes changes in the magnetic field. The change occurs as the metallic teeth and open spaces on the impulse wheel pass the sensor.

In Figure 2-15, the impulse wheel rotates at wheel speed 1.) as the tooth passes the sensor=the magnetic core increases, there is high magnetic flux 2.) this increases the signal amplitude. As the impulse wheel continues at wheel speed, 3.) the gap passes the sensor, which causes the magnetic field to collapse, which in turn creates low magnetic flux 4.) Signal amplitude is decreased, which completes the cycle for a complete signal.

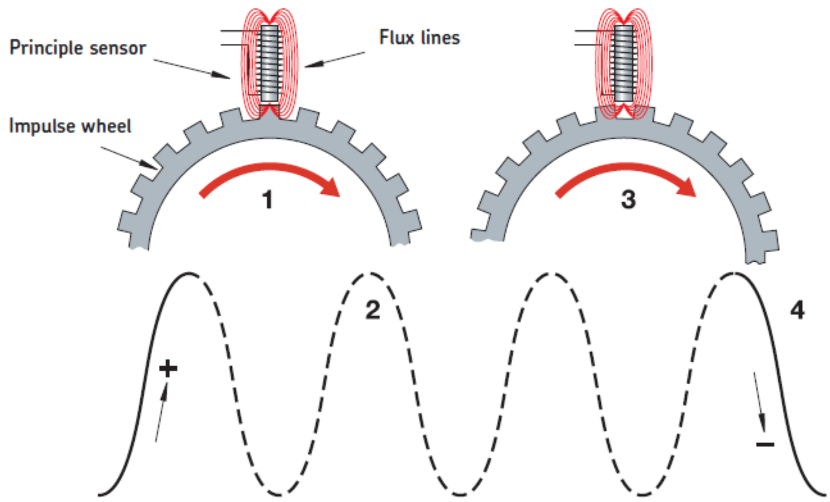

Figure 2-15: Principle of the passive wheel speed sensor

Table 2-1: Actuators comparison

	Electric motor	Friction brake
Torque	$T_m = K_t \cdot I$	$T_b = r_d \gamma \cdot F_\perp$
Dynamics	Fast	Slow
Max torque	Low	High

The sensor and impulse wheel are exposed to a harsh environment, including temperature extremes, vibration, grit and dirt, water, etc., all of which can affect the system efficiency.

2-4 Short Conclusion

This chapter first gives a top layer overview of the model blocks, then introduces the wheel force dynamics, two important brake actuators (hydraulic brake and electric motor brake) and wheel speed sensors. In each part, we analyze its control logic and show some simulation blocks in this project design. A short comparison between these two actuators is shown in Table 2-1. The max torque of electric motor is usually around 200 Nm, not big enough to cover all required brake torque. The max torque of friction brake is much bigger, more than 1000 Nm.

In the hybrid electric vehicles, the regenerative braking can not be used for many reasons such as high state of charge or high temperature of the battery to increase the battery life. So that is why the torque generated by the motor needs to work with the friction braking torque together. In short, the direction of development of modern cars is modular, integrated, mechatronics, and ultimately realize automotive steer by wire system.

Chapter 3

Anti-lock Braking System

Anti-lock braking system (ABS) technology has been used in the automotive industry since the 1980's [14] and is implemented in most modern cars today. According to the Bosch website, 76 percent of all new vehicles were equipped with ABS in 2007 and it has become a standard equipment for passenger cars in the EU, the U.S. and Japan.

There are two reasons for installing an ABS system in a car. The first objective is to avoid wheel lock-up and preserve the tyre ability or produce a lateral force, and thus vehicle maneuverability. Furthermore, the wheel slip is kept in a neighborhood of the point that maximizes the tyre force in order to minimize the vehicle's braking distance.

In braking control system, two output variables are usually considered for regulation purposes: wheel deceleration and wheel slip. These output variables have characteristics that are somehow complementary.

Approaches based on wheel slip regulation [9][15][16] have several nice features: they are often based on clear mathematical background and the torque applied to the wheel converges to a fixed value. However, their usage nevertheless confronts us with two difficulties. Firstly, it is not always very clear how to estimate the wheel slip precisely due to the fact that the vehicle speed is difficult to measure. Secondly, the value of wheel slip λ^* for which the longitudinal tyre force is maximal is general unknown and not easy to estimate in real-time.

Approaches based on wheel deceleration thresholds [8][17] have quite interesting properties too: they are very robust with respect to friction coefficient changes and can keep the wheel slip in a neighborhood of the optimal point, without using explicitly the value of the optimal set point. But a particularly unpleasant characteristic of these approaches is that they are often based on heuristic arguments, and thus tuning the thresholds involved in this kind of algorithms might be a difficult task.

In this thesis, we use wheel deceleration control, cooperating work with the electric motor and the performance of regenerative braking is tested based on the reasonable thresholds setting.

3-1 Wheel Deceleration Control

Wheel deceleration is the controlled output traditionally used in ABS, since it can be easily measured with a simple wheel sensor. By calling back the previous chapter 2, the quarter car model used in this thesis is represented by:

$$J\dot{\omega} = -RF_x + T \tag{3-1}$$

The vehicle is supposed to brake with the maximal constant deceleration a_x^* allowed by road conditions, which is $a_x^* = -\mu(\lambda^*)g$. In other words

$$\dot{v_x} = a_x^*$$

The vertical forces F_z on the front and rear axles are assumed constant and equal to those one would have at equilibrium for this constant deceleration a_x^*. The front and rear wheel dynamics are then assumed decoupled.

Let $\lambda^* = -\lambda_0$ be the optimal negative wheel slip, such that $\mu^{'}(\lambda^*) = 0$. If we define the wheel slip offset x_1 and the wheel acceleration offset x_2 by

$$x_1 = \lambda - \lambda^* \tag{3-2a}$$
$$x_2 = r\dot{\omega} - a_x^* \tag{3-2b}$$

we obtain the following dynamical system:

$$\dot{x_1} = \frac{1}{v_x}(x_2 - (\lambda^* + x_1)a_x^*) \tag{3-3a}$$
$$\dot{x_2} = -\frac{a}{v_x}\bar{\mu}^{'}(x_1)(x_2 - (\lambda^* + x_1)a_x^*) + u \tag{3-3b}$$

where $a = \frac{R^2}{J}F_z$ and $u = \frac{R}{J}\dot{T}$. The function $\bar{\mu}(\cdot)$ is defined as

$$\bar{\mu}(x) = \mu(\lambda^* + x) - \mu(\lambda^*).$$

3-2 Five-phase Hybrid Control Strategy

To ensure the robustness, the choice can be made between classical robust control and hybrid robust control. The first methods often depend on a certain model and work with deterministic rules, while hybrid control uses predetermined thresholds for control. By using the methods based on the deterministic rules, the action can be relatively easily explained and robustness can be proven, but it will be difficult to obtain the optimum value. Using hybrid control, a suboptimal region will result from this type of control. In hybrid control, robustness can be guaranteed through methods such as limit cycle analysis, if increasing the number of hybrid rules, the control performance can come very close to the optimum braking value. So in this thesis, we choose the five-phase ABS control algorithm [17].

For ABS regulation, the control objective is to keep the unmeasured variable x_1(slip offset) in a small neighborhood of zero, with a control u that only uses the measured variable $x_2 = R\dot{\omega} - a_x^*$.

3-2-1 Simplified First Integrals

Consider a dynamics system

$$\dot{x} = f(x), where \quad x \in \mathbb{R}^n.$$

For this system, a first integral is a function of the state $I(x)$ that remains constant along the trajectories of the system. That is, such that

$$\frac{d}{dt} I(x(t)) = \sum_{i=1}^{n} \frac{\partial I}{\partial x_i}(x(t)) f_i(x(t)) = 0.$$

Thus, on any time interval $[t_0, t_1]$, we have

$$I(x(t)) = I(x(t_0)), \tag{3-4}$$

for all $t \in [t_0, t_1]$.

In the particular case of two-dimensional dynamical systems, first integrals can be used to compute the phase-plane evolution of the system. Indeed, the evolution of any of the two variables of the system can be deduced from the other variable using (3-4).

In this project, our control variable is brake torque, based on the first integral solutions, we analysis the torque variations depicted as control actions in each phase respectively.

Constant torque When the control variable is such that $u = 0$, the torque applied to the wheel remains constant. Therefore, the torque itself is a first integral.

Large torque variations When $u \neq 0$, to find exact first integral is difficult. Nevertheless, for controls having the following particular form $u = u_0/R\omega$ with u_0 large enough, an approximative description of the system's evolution still can be obtained.

Small torque variations This variation corresponds to the phase 5 in Figure 3-2, during this phase the brake torque increased slowly. For controls having the particular form $u = u_0 x_2/R\omega$ with u_0 small enough, an approximative description of the system's evolution can still be obtained.

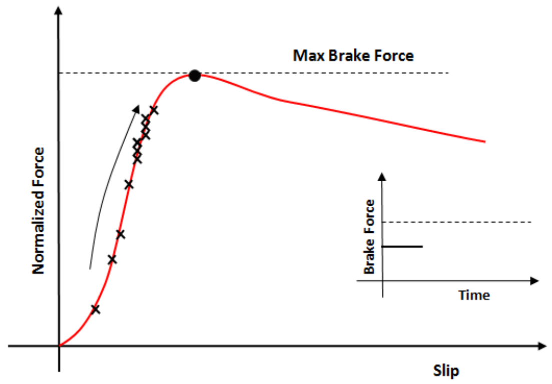

(a) The braking force is immediately applied of which stability is guaranteed deterministically

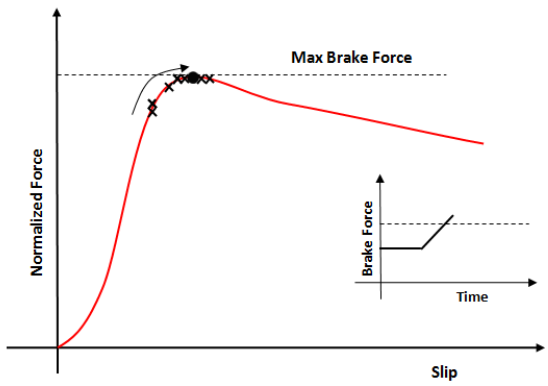

(b) The braking force keeps increasing

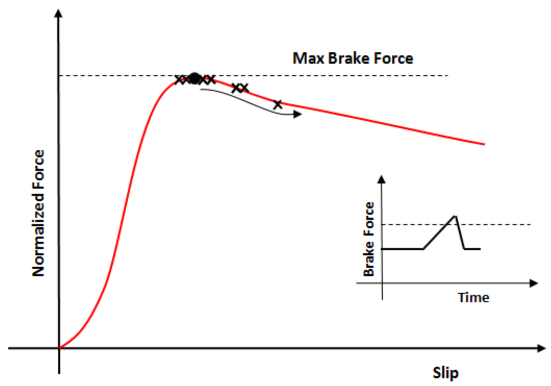

(c) When instability region is reached, braking force is set to decrease quickly

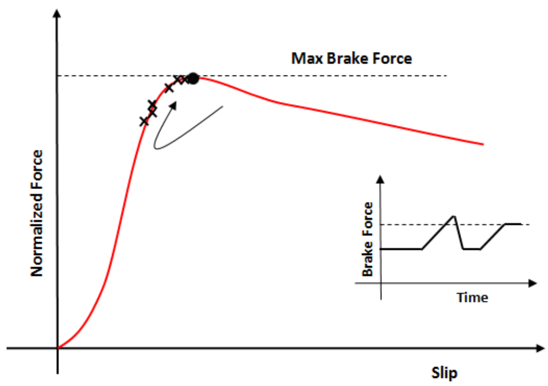

(d) Once wheel slip is in the stable region, holding the brake pressure

Figure 3-1: The different steps taken by the ABS controller. The highest guaranteed braking force is applied immediately. Once this is reached, the force is slowly increased until instability occurs. Braking force is consequently reduced. The last known stable braking force is applied as soon as wheel sip is in the stable region

3-2-2 The Algorithm

The ABS control process is that by increasing, decreasing or holding the brake pressure to avoid the wheel lock up and optimize the braking distance. By calling back the previous chapter 2, we want to keep the slip value in a optimal region, so if the value of λ is smaller than the optimal value λ^*, the system always stay in the stable region, our ABS controller will not be used. Once λ exceeds the optimal value λ^*, the ABS controller will start to work immediately. Figure 3-1 gives a graphical interpretation of the ABS control process when finding the optimal braking force.

Actually, in the real driving condition, the value of λ is difficult to measure, so we use a deceleration threshold which is measurable. It means that the deceleration threshold should be larger than the maximal constant deceleration. In this simplified model,

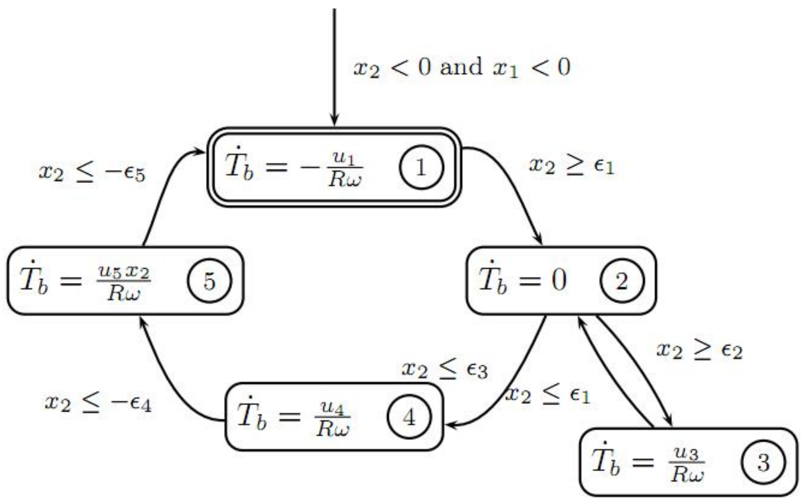

Figure 3-2: The five-phase ABS regulation logic

the maximal constant deceleration a_x^* allowed by road conditions is described as $a_x^* = \mu(\lambda_0)g$. Obviously, for different road conditions the value of λ_0 is different, so the value of a_x^* is different. We need to use adaptive a_x^* to the current road condition, but this is very difficult. Therefore, we use an empirical value for the controller design which is equal to 0.25. By calling back the previous function $\mu(\lambda)$ we can get the value of a_x^* as $-10.78\ m/s^2$.

The choice has been made to build a hybrid controller with deterministically determined thresholds. In this fashion, deterministic design is the basis of the controller and hybrid control is used to fine tune the system and further increase performance. The basic ABS control regulation logic that we will consider is described on Figure 3-2. As shown in this figure, there exist five phases and each phase has its own trigger condition. As soon as one of these guard conditions that determine a discrete transition from the current phase becomes true, the algorithm will switch to the next phase and change the control action immediately [18][19].

PHASE 0 Once $x_1 < 0$ and $x_2 < 0$, it means that the wheel has entered the unstable domain: if the brake pressure is maintained constant then the wheel will lock.

PHASE 1 We rapidly decrease brake torque by taking $\dot{T}_b = -u_1/R\omega$ until $x_2 \geq \epsilon_1$. The aim of this phase is to change the sign of the wheel's angular acceleration by decreasing brake torque rapidly. The consequence of this brake pressure decrease is that the wheel slip will first stop increasing and then will start decreasing.

PHASE 2 As soon as $x_2 \geq \epsilon_1$, we maintain a constant brake torque. The variable x_2 will first increase while $x_1 < 0$; and then decrease once $x_1 > 0$ (provided that Phase 3 is not triggered before). All along Phase 2, we have $x_2 < \epsilon_2$ and $x_2 > \epsilon_3$. Indeed, Phase 3 is triggered when $x_2 > \epsilon_2$, while Phase 4 is triggered when $x_2 \leq \epsilon_3$. The practical aim of this phase is to detect whether we are in the stable or in the unstable region wheel dynamics.

PHASE 3 In this phase, we rapidly increase brake torque until $x_2 \leq \epsilon_1$, which will trigger the second phase of the algorithm. Phase 2 and Phase 3 will then alternate until $x_2 \leq \epsilon_3$, which will trigger the fourth phase. From a physical point of view, the aim of this phase is to prevent the wheel from returning too far into the stable region (which would increase the braking distance).

PHASE 4 As soon as $x_2 \leq \epsilon_3$, we rapidly increase the brake torque until $x_2 \leq -\epsilon_4$, which will trigger the fifth phase. Once this phase has been triggered, we know that we are in the stable region of the wheel dynamics. We can thus increase the brake pressure in order to change the sign of wheel deceleration and increase slip again.

PHASE 5 The aim of this phase is to detect that the wheel has reached the unstable region, and it is necessary to start again the algorithm from the beginning.

Note that these guard conditions only depend on the value of the measured variable wheel acceleration offset $x_2 = R\dot{\omega} - a_x^*$.

3-3 Algorithm Tuning

In the brake pressure dynamics, the hydraulic line and the servo-valve used to control the pressure in the disk brake limit the performance of the actuation. In a first approximation, the controlled valve will introduce a second-order dynamics and the hydraulic line a transport time delay between the desired and the actual brake pressure, the influence of these factors should be taken into account before designing a ABS system.

The parameters chosen in this tuning work are: pure time delay set as 7 ms and the second order system of dynamic response with a natural frequency of 60 Hz and a damping factor of 0.33.

In five-phase ABS control algorithm, nine parameters need to be chosen: the wheel deceleration threshold ϵ_i and the brake pressure derivatives u_i.

In the simulation analysis, we used symmetric thresholds (that is $\epsilon_5 = \epsilon_1$ and $\epsilon_4 = \epsilon_3$)which are recommended in [17]. Choosing symmetric thresholds usually gives better results and simplifies considerably the tuning of the control parameters u_i.

Before we start to analyze the sensitivity of these parameters, three main different trends of tuning parameter need to be introduced. Usually when we set a cost function J and through changing the value of input variable x, there exists three different trends which is shown in Figure 3-3. For trend 1, by increasing the variable x, the value of cost function J is decreasing, and according to the trend direction, the smaller the better. However, for trend 2, it is just the opposite. For trend 3, we can see that the optimal value is a convergence on both sides.

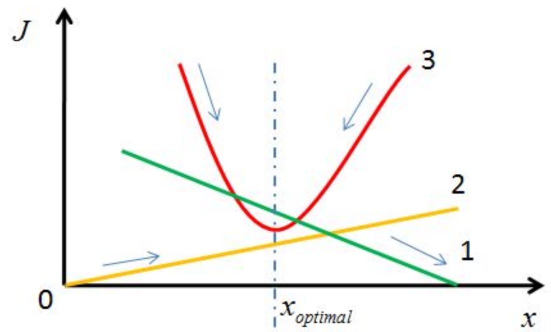

Figure 3-3: The trends for cost function

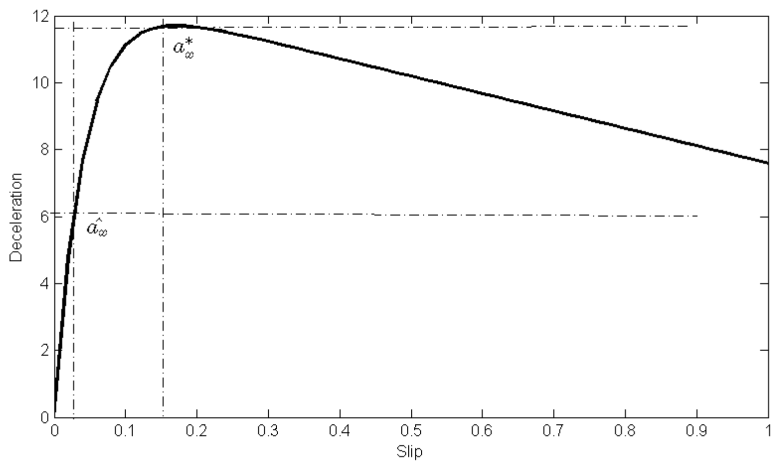

Figure 3-4: $a - \lambda$ map

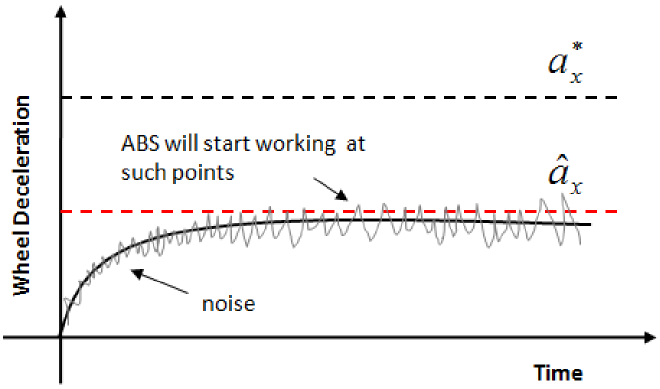

Figure 3-5: The noise effects. Due to the noise effects, at some points the actual wheel deceleration exceed threshold $\hat{a_x}$ which will result in ABS start working

3-3-1 Sensitivity Analysis of Tuning Parameters

Actually, once the vehicle steps into the unstable region, the wheel will lock up immediately, so the value of a_x^* can not be set too large. However when setting this value too small, here we use $\hat{a_x}$ to estimate the value of a_x^*, from Figure 3-4 we can see that $\hat{a_x} < a_x^*$, the correspond maximum braking torque of $\hat{a_x}$ is much smaller than the maximum torque of a_x^*, this will lead to a long braking distance. In practice, the roads are uneven, also some sensing errors and other noise effects result in the deceleration value close to the threshold, this can be seen in Figure 3-5. At some points, it will lead to the wrong control action, the ABS start to work where actually the deceleration is below the threshold. In order to test the sensitivity of acceleration and deceleration thresholds setting, we first choose an average deceleration threshold and test the ABS performance by using a large and a small acceleration threshold separately then vice versa.

- ϵ_1 This threshold is used to determine when phase 2 is triggered. If $x_2 \geq \epsilon_1$, we stop decreasing the brake torque and start to maintain a constant brake torque. We choose three different values of ϵ_1, which are 11 m/s^2, 20 m/s^2, 90 m/s^2 respectively.

  For the small value, $\epsilon_1 = 11\ m/s^2$, the results are shown in Figure 3-6(a) and Figure 3-6(b), we can see that the wheel lock up gradually, the reason is that because ϵ_1 is small, so the guard condition can be triggered easily and step into the next phase, the decreasing torque is not sufficient, then the slip is gradually increasing which leads to the wheel lock up.

  For the mid value, $\epsilon_1 = 20\ m/s^2$, the results are shown in Figure 3-6(c) and Figure 3-6(d), we can see that the ABS control loop works well.

  For the large value, $\epsilon_1 = 90\ m/s^2$, the results are shown in Figure 3-6(e) and Figure 3-6(f), we can see that after reaching the first phase, the system can not trigger the guard condition anymore to step into the next phase, because the

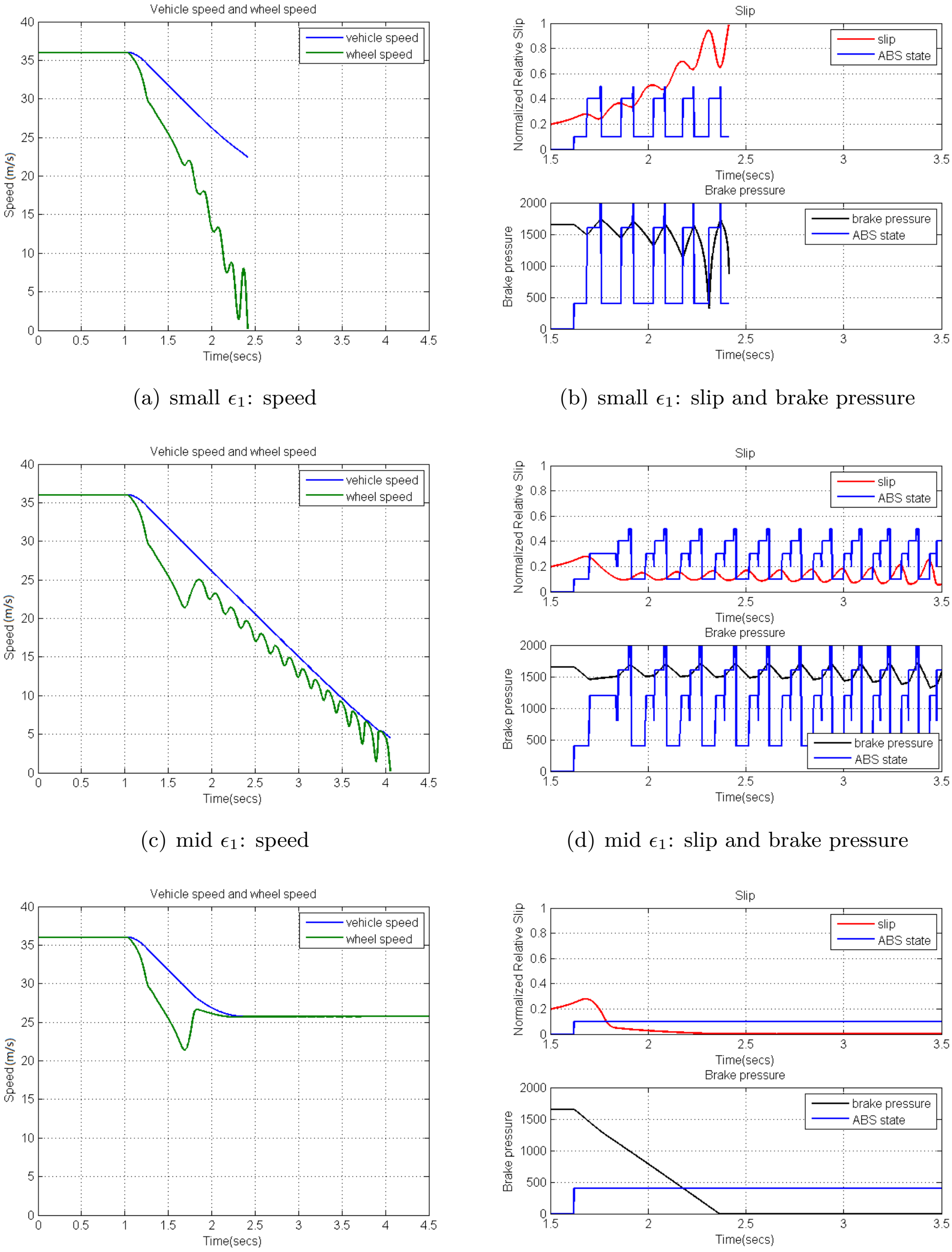

(a) small ϵ_1: speed

(b) small ϵ_1: slip and brake pressure

(c) mid ϵ_1: speed

(d) mid ϵ_1: slip and brake pressure

(e) large ϵ_1: speed

(f) large ϵ_1: slip and brake pressure

Figure 3-6: ϵ_1 effect analysis threshold setting is too large. So the ABS works in phase 1, decreasing the braking torque until zero.

- $\epsilon_{3,4}$ As soon as $x_2 \leq \epsilon_3$, we rapidly increase the brake torque in phase 4 and until $x_2 \leq \epsilon_4$, which will trigger the fifth phase. We choose three different values of ϵ_1, which are $11\ m/s^2, 20\ m/s^2, 90\ m/s^2$.

  For the small value, $\epsilon_{3,4} = 11\ m/s^2$, according to the description of previous phase 4, we know that once phase 4 has been triggered, we are in the stable region of the wheel dynamics, we can thus increase the brake pressure in order to change the sign of wheel deceleration and increase slip again. However, if this threshold is set small, it means that the brake torque will start increasing at a very small slip value which is much smaller than the optimal value (which would increase the braking distance). It can be seen in Figure 3-7(b) and Figure 3-7(d), the average slip value in Figure 3-7(b) is much smaller than the one in Figure 3-7(d).

  For the mid value, $\epsilon_{3,4} = 20\ m/s^2$, from Figure 3-7(c) and Figure 3-7(d) we can see it works better than the small value of $\epsilon_{3,4}$.

  For the large value, $\epsilon_{3,4} = 90\ m/s^2$,from Figure 3-7(e) we can see the wheel lock up gradually, because the threshold of $\epsilon_{3,4}$ is large, then the phase 4 can be triggered more easily than before, the decreasing torque in phase 1 is not sufficient, the slip is gradually increasing which leads to the wheel lock up. Here we have to pay attention to that we use symmetric switching threshold, $\epsilon_3 = \epsilon_4$. When $\epsilon_{3,4}$ are setting large, the phase 4 can be triggered more easily (ϵ_4 *is large*), in another side, it is difficult to get out phase 4 (ϵ_3 *is large*), so the algorithm will stay in phase 4 for a long time.

Therefore, it is essential that setting an appropriate acceleration threshold to ensure the reliability of ABS regulation logic, also it is necessary to take comprehensive consideration of thresholds selecting and pressure derivative setting. Now we study the effects of pressure derivative setting.

- u_1 This parameter is used in phase 1. Once the driver ask for a large torque to brake the wheel, and the wheel may have a locking trend, we rapidly decrease the brake torque by taking $\dot{T}_b = -u_1/R\omega$ to avoid wheel lock up. In order to study the sensitivity of u_1, here we choose three different values of u_1, which are $u_1 = 5.6 \times 10^3\ pa, u_1 = 5.6 \times 10^4\ pa, u_1 = 5.6 \times 10^5\ pa$.

  For the small value, $u_1 = 5.6 \times 10^3\ pa$, from Figure 3-8(a) we can see that the wheel lock up quickly. Because $\dot{T}_b = -u_1/R\omega$ is not large enough to supply a fast decreasing pressure derivative, then the wheel lock up.

  For the mid value, $u_1 = 5.6 \times 10^4\ pa$, from Figure 3-8(c) and Figure 3-8(d) we can see that as soon as phase 1 triggered, by decreasing the brake torque, it prevents the wheel from locking up successfully.

  For the large value, $u_1 = 5.6 \times 10^5\ pa$, from Figure 3-8(e) and Figure 3-8(f) we can see that our five phase ABS regulation logic works, but because of large u_1, the decreasing torque derivative is too big, in some periods of time, the slip is almost

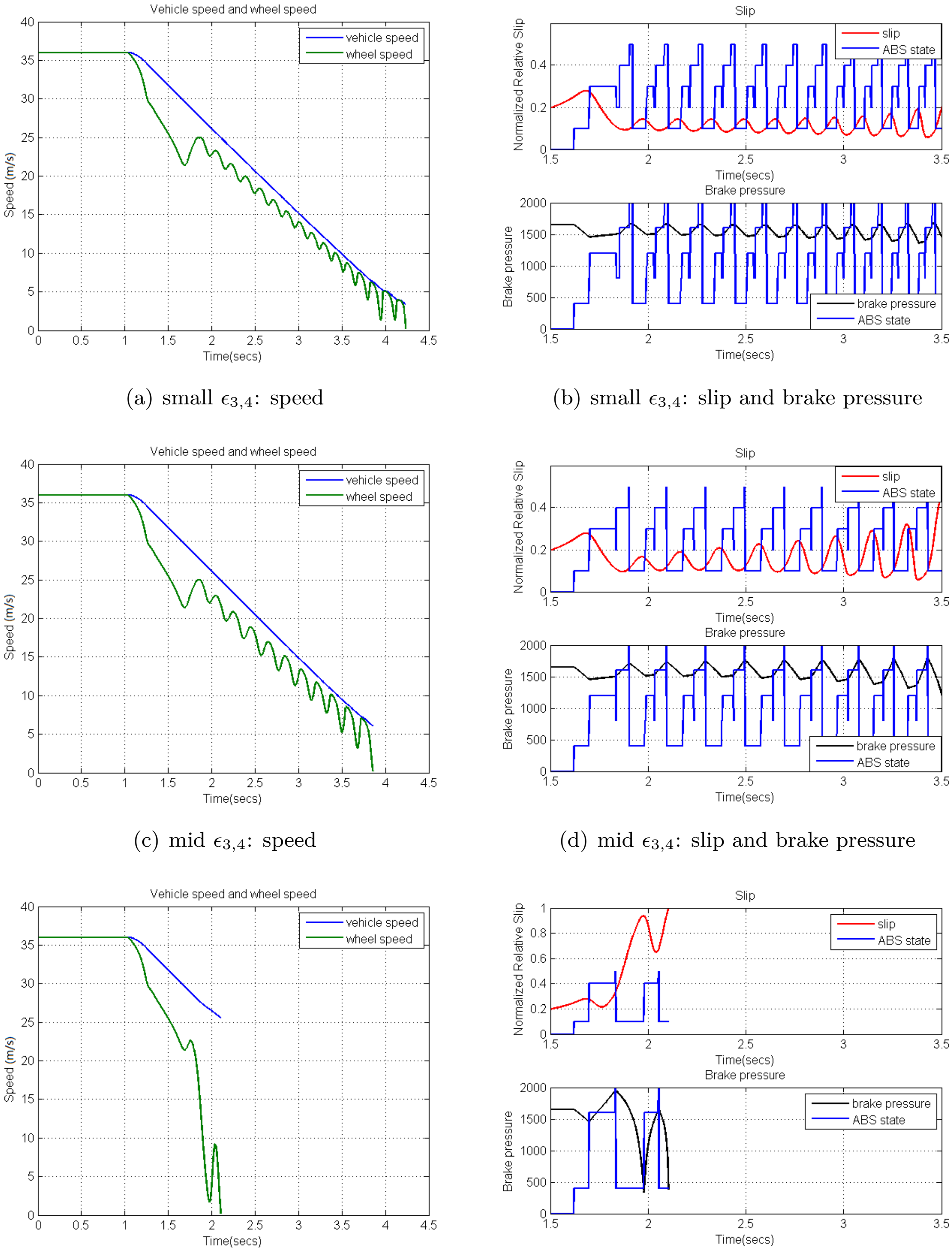

(a) small $\epsilon_{3,4}$: speed

(b) small $\epsilon_{3,4}$: slip and brake pressure

(c) mid $\epsilon_{3,4}$: speed

(d) mid $\epsilon_{3,4}$: slip and brake pressure

(e) large $\epsilon_{3,4}$: speed

(f) large $\epsilon_{3,4}$: slip and brake pressure

Figure 3-7: $\epsilon_{3,4}$ effect analysis

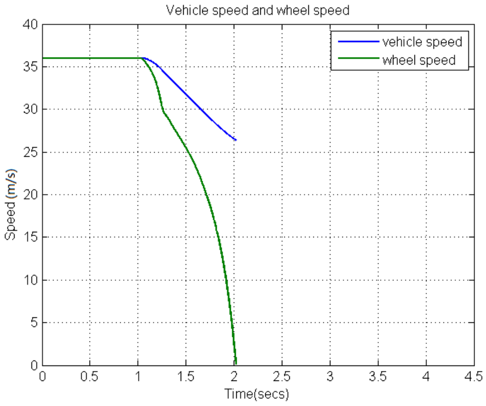

(a) small u_1: speed

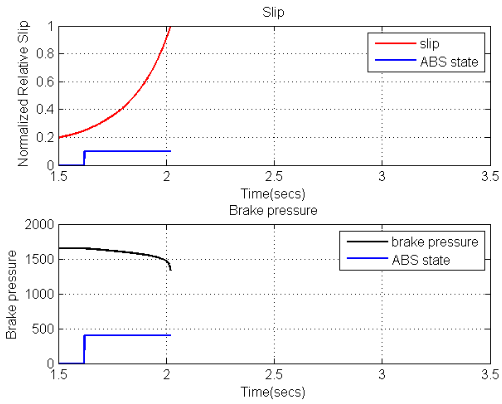

(b) small u_1: slip and brake pressure

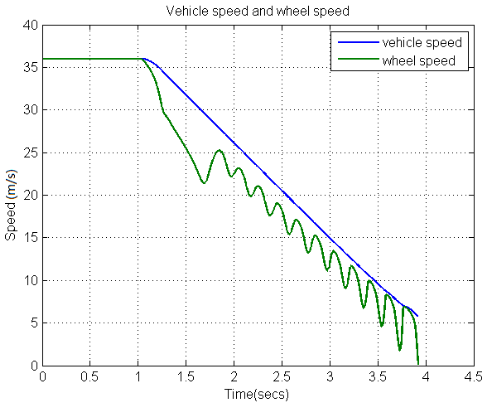

(c) mid u_1: speed

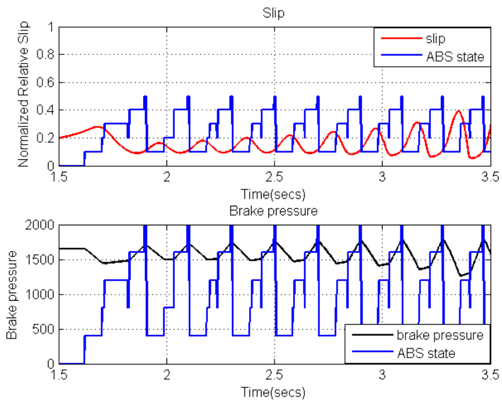

(d) mid u_1: slip and brake pressure

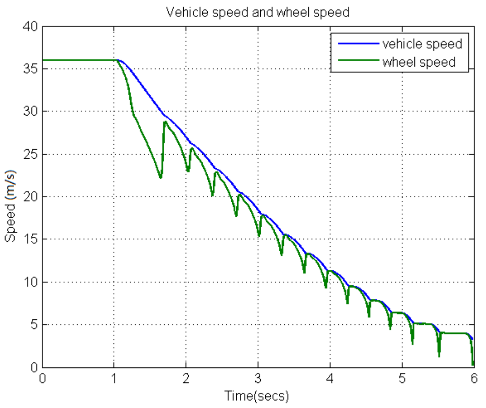

(e) large u_1: speed

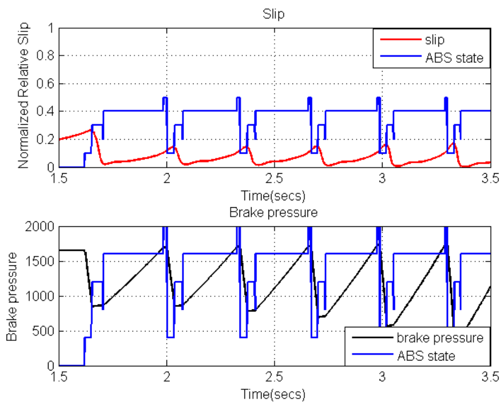

(f) large u_1: slip and brake pressure

Figure 3-8: u_1 effect analysis

equal to zero (which will lead to a long braking distance). This can be seen in Figure 3-8(f).

- u_3 The value of u_3 used in Phase 3 is to prevent the wheel from returning too far into the stable region.

  For the small value, $u_3 = 800\ pa$, in phase 3 the increased torque is small, it can not well prevent the wheel from returning too far into the stable region, then the braking torque will stay in small slip region (much lower than the optimal value) longer time which will lead to a longer braking distance. This can be seen in Figure 3-9(a) and Figure 3-9(b).

  For the mid value, $u_3 = 2.5 \times 10^4$, we can see that the brake pressure in trough region (ABS state 3) shown in Figure 3-9(d) is larger than the result shown in Figure 3-9(b), it is better than before.

  For the large value, $u_3 = 5 \times 10^5\ pa$, from Figure 3-9(e) we can see the wheel lock up quickly, because after we rapidly decrease the brake torque in phase 1, then the guard condition of phase 3 is triggered, by using a big value of u_3, the value of $\dot{T}_b = u_3/R\omega$ is large, so the brake torque will increase too much then the wheel lock up quickly.

- u_4 This parameter is used in phase 4, once the fourth phase is triggered, we can increase the brake torque by taking $\dot{T}_b = u_4/R\omega$. Here we also use three values to test its sensitivity, the values are $8 \times 10^3\ pa, 8 \times 10^4\ pa, 8 \times 10^5\ pa$.

  For the small value, $u_4 = 8 \times 10^3\ pa$, because the increased torque is very small, from Figure 3-10(b), we can see that the system stays in state 4 for a long time. If the wheel returns too far away from the stable region, and in phase 4 it can not get a quick increasing torque, then the system will work in a small slip region too long, which means the braking distance will become longer.

  For the mid value, $u_4 = 8 \times 10^4\ pa$, from Figure 3-10(c) and Figure 3-10(d), we can see that our ABS works well.

  For the large value, $u_4 = 8 \times 10^5\ pa$, the wheel lock up quickly which is shown in Figure 3-10(e). Because the increase torque in phase 4 is too large then the wheel lock which can be seen in Figure 3-10(f).

- u_5 This parameter is used in phase 5. The aim of this phase is to detect that the wheel has reached the unstable region, and it is necessary to start again the algorithm from the beginning. If too big value of u_5 is chosen (here we use $5 \times 10^4\ pa$), the wheel might lock, this can be seen in Figure 3-11(e) and Figure 3-11(f).

  Then we use other two different values to check its performance, a small value $50\ pa$ and a mid value $2 \times 10^3\ pa$. The results are shown in Figure 3-11, we can see that the average slip value shown in Figure 3-11(d) is slightly larger than the value shown in Figure 3-11(b). So the results show that the performance of parameter u_5 is not so sensitive to a smaller value region.

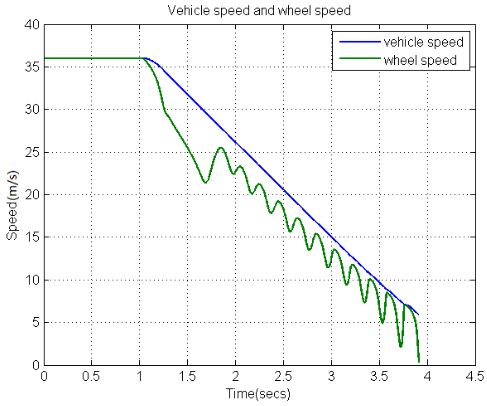

(a) small u_3: speed

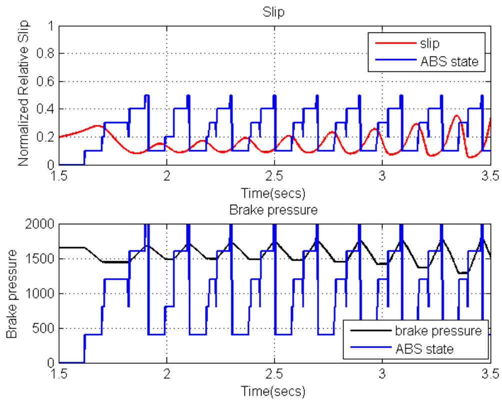

(b) small u_3: slip and brake pressure

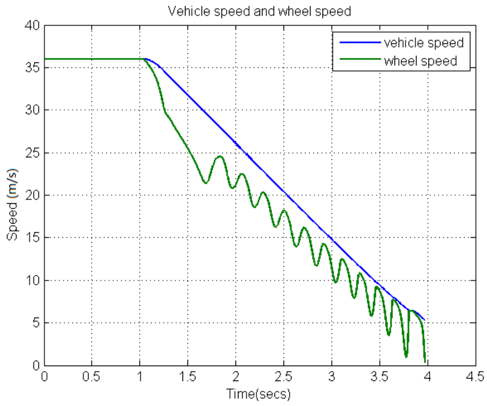

(c) mid u_3: speed

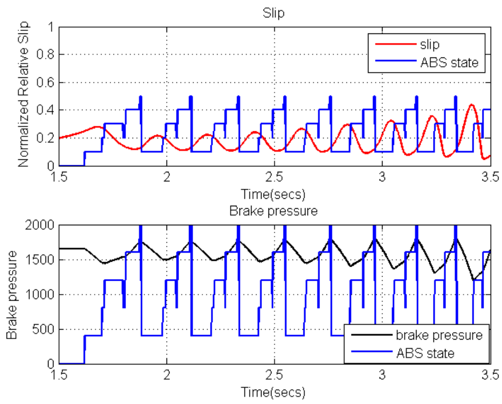

(d) mid u_3: slip and brake pressure

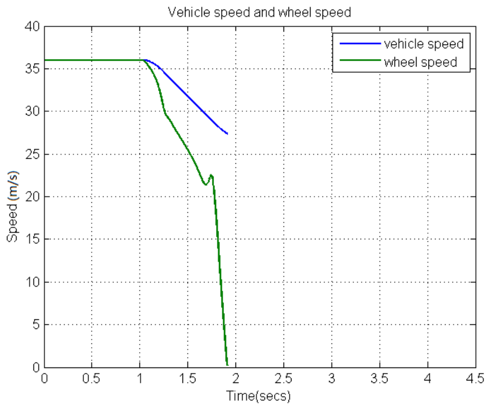

(e) large u_3: speed

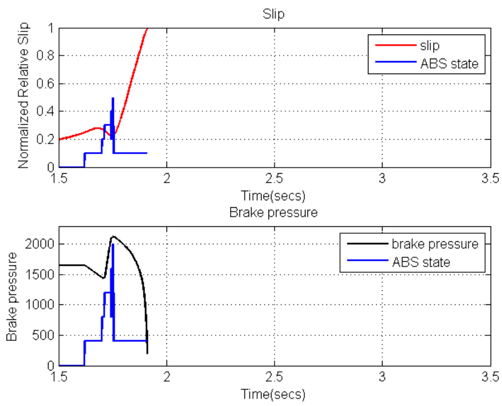

(f) large u_3: slip and brake pressure

Figure 3-9: u_3 effect analysis

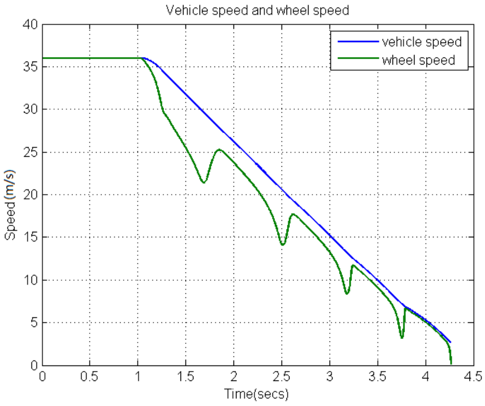

(a) small u_4: speed

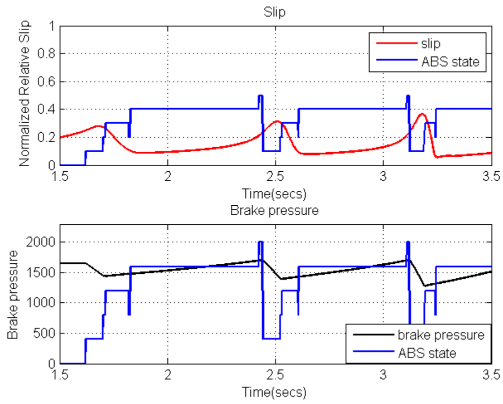

(b) small u_4: slip and brake pressure

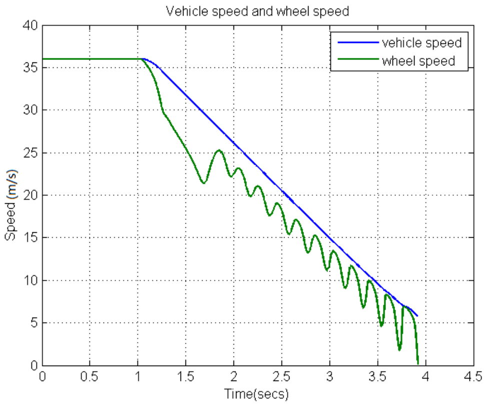

(c) mid u_4: speed

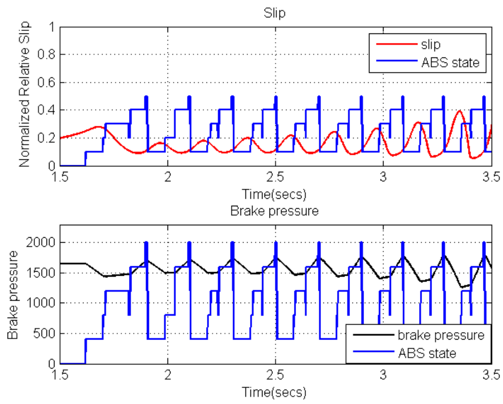

(d) mid u_4: slip and brake pressure

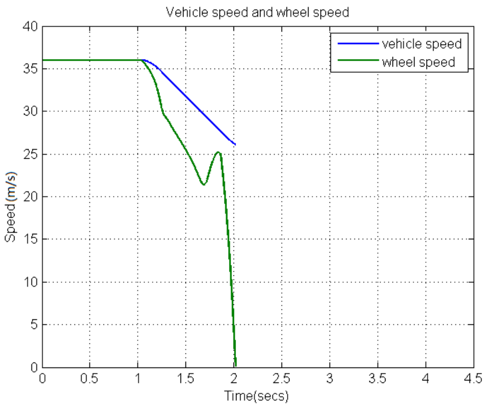

(e) large u_4: speed

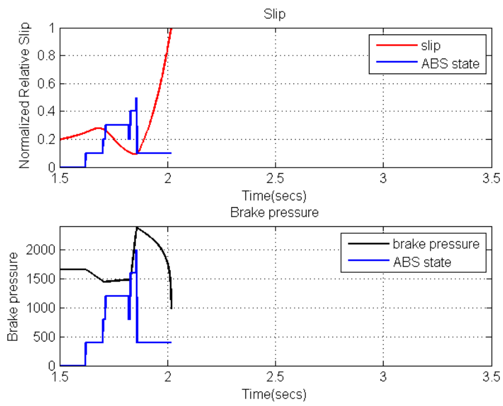

(f) large u_4: slip and brake pressure

Figure 3-10: u_4 effect analysis

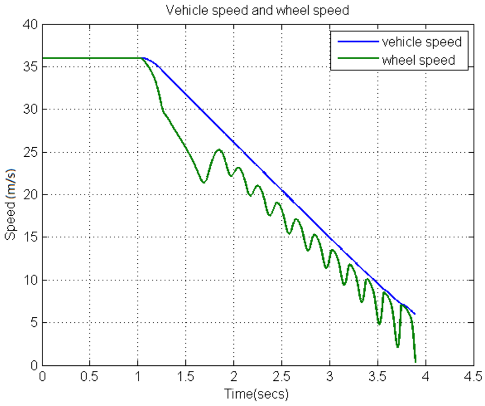

(a) small u_5: speed

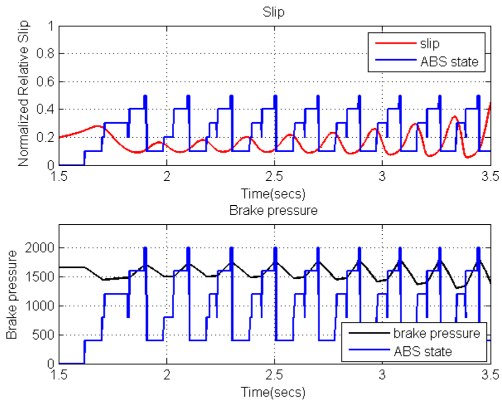

(b) small u_5: slip and brake pressure

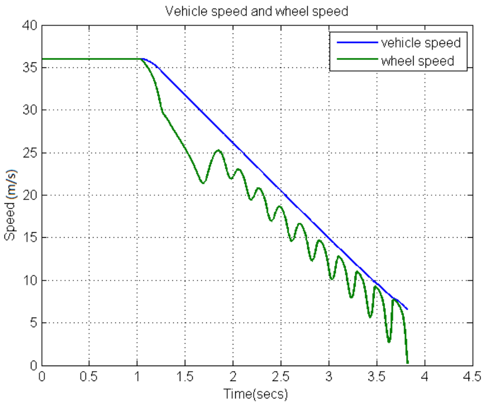

(c) mid u_5: speed

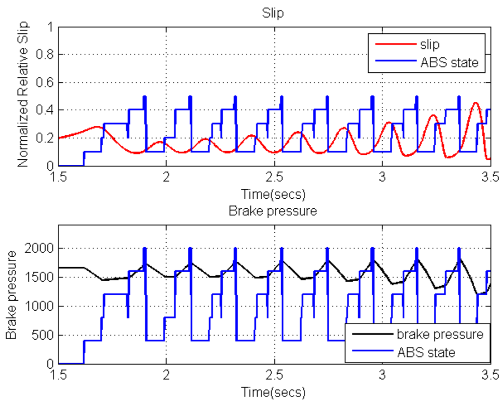

(d) mid u_5: slip and brake pressure

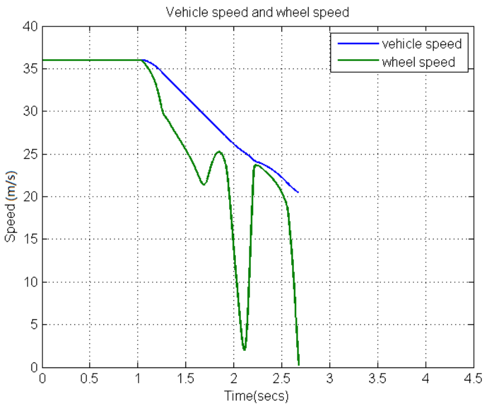

(e) large u_5: speed

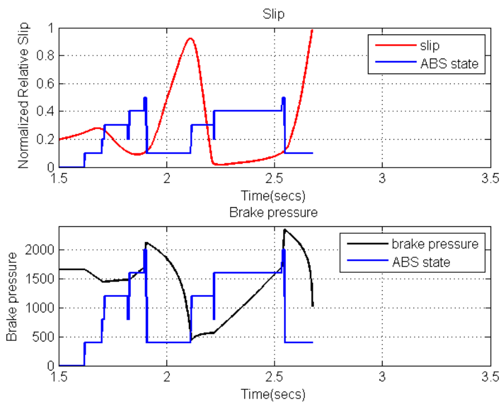

(f) large u_5: slip and brake pressure

Figure 3-11: u_5 effect analysis

3-3-2 Optimal Tuning

As we know, the main objective of ABS is to maintain the maximum brake force to reduce the brake distance. So we choose the braking distance as the cost function to define the optimality, however from the previous figures we can see that the wheel always lock up before the vehicle speed is equal to zero. Because we consider the vehicle speed v as a slow varied parameter which does not affect the stability and minimum-phase properties but it has effect on scaling the wheel dynamics. As the velocity is decreased, the dynamics gets faster, this can be seen in chapter 2. By using adaptive threshold setting, the situation can be improved. So in this thesis, we compare the braking distance from the initial braking speed to 7 m/s, then the cost function can be defined as below:

$$d = \int_{v_0}^{7} v dt$$

First we select some reasonable deceleration thresholds, then we tune the pressure derivative parameters based on the analysis of parameters sensitivity above, the optimal values we choose as: $\epsilon_{1,5} = 20\ m/s^2, \epsilon_2 = 25\ m/s^2, \epsilon_{3,4} = 14\ m/^2$ and $u_1 = 5.6 \times 10^4\ pa, u_2 = 0, u_3 = 8 \times 10^3\ pa, u_4 = 8 \times 10^4\ pa, u_5 = 220\ pa$. The results are shown in Figure 3-12 and the braking distance is 60.47 m.

3-3-3 The Effect of Transport Time Delay

The main difference between the ideal braking system and the practical braking system is the transport time delay. This time delay is caused by the following reasons:

- The delay generated by the brake transmission medium. For example, in the hydraulic brake system due to the fluid component, the braking fluid transmit to the wheel mask cylinder need some time.
- The transmission delay of brake actuator systems. For example, to overcome the brake friction pair dead zone and brake clearance will take some time.

During this test, first we keep the previous optimal tuning thresholds fixed and just change the time delay, then for each time delay, according to our cost function, we compute the braking distance. The test results are shown in Table 3-1 and Figure 3-13(a). We can see that with time delay increasing, the braking distance is increasing.

Obviously, the time delay affects negatively the ABS braking performance. As shown in Figure 3-14, the system reaches the deceleration threshold at point A, it should begin to decrease the brake torque, however the brake torque will keep increasing to the point B which is caused by the time delay. Now if the deceleration threshold set to large and the road coefficient is low, the wheel will be locked possibility in AB time period. The same for the decreasing process, the braking torque reaches the acceleration threshold at point C, the brake torque will keep decreasing for a short while due to the time

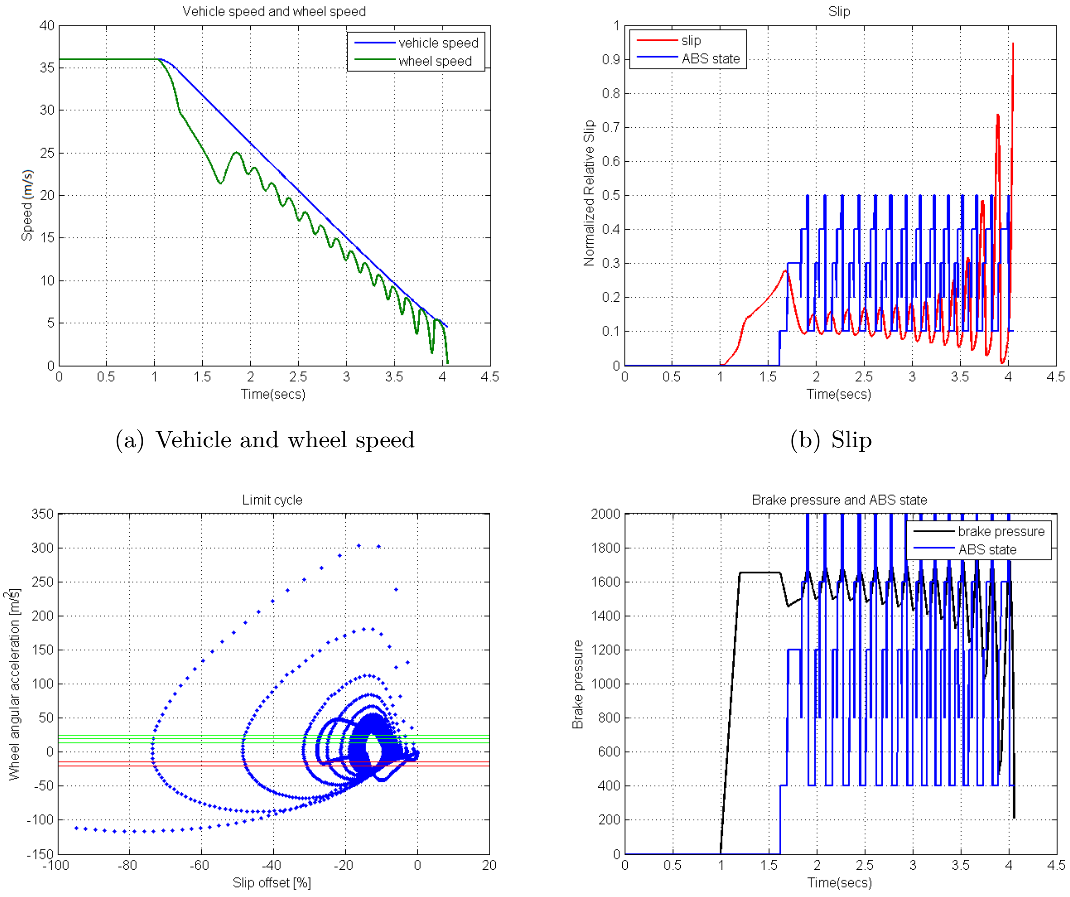

(a) Vehicle and wheel speed (b) Slip

(c) Limit cycle (d) Brake pressure

Figure 3-12: Optimal tuning results

Table 3-1: The effect of time delay

Delay	Braking distance
7 ms	60.47 m
11 ms	60.74 m
13 ms	60.87 m
15 ms	61.28 m

Table 3-2: The effect of bandwidth

Frequency	Braking distance
60 Hz	60.47 m
55 Hz	60.76 m
50 Hz	61.00 m
45 Hz	61.56 m

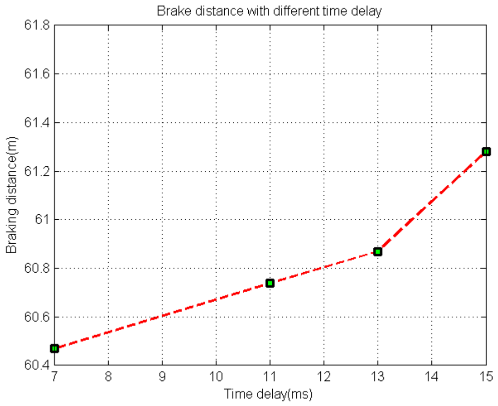

(a) Brake distance with different time delay

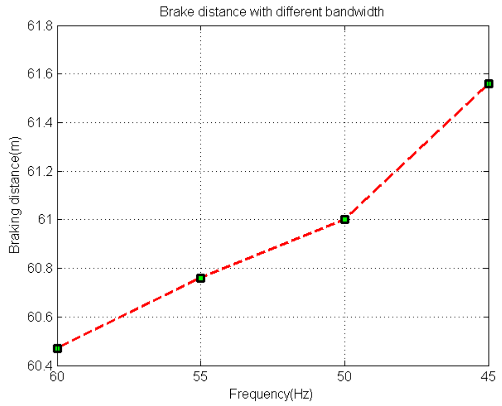

(b) Brake distance with different bandwidth

Figure 3-13: Braking distance

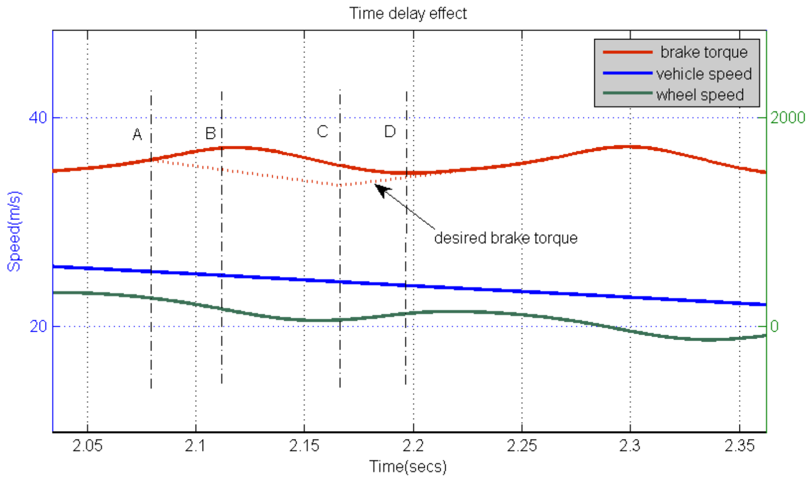

Figure 3-14: Time delay analysis

delay. During this short time, if the wheel rotational inertia is small, the wheel speed will recover too much which will make braking distance long.

Taking these factors into account, we know that the actual braking system is different to the theoretical braking system. So if the time delay is large, we need to choose a small deceleration threshold in order to avoid the wheel locked.

3-3-4 The Effect of Bandwidth

In the previous section we already analyzed the effect of time delay, in order to check if the change of bandwidth will cause the same response, now we study the effect of bandwidth. The values of bandwidth tested here are 60 Hz, 55 Hz, 50 Hz, 45 Hz, the results can be seen in Figure 3-13(b) and Table 3-2.

Table 3-3: Parameters list

Surface	θ_{r1}	θ_{r2}	θ_{r3}
Asphalt, dry	1.28	23.99	0.52
Asphalt, wet	0.86	33.82	0.35
Cobblestone, dry	1.37	6.46	0.67
Snow	0.19	94.13	0.06

The results demonstrate that decreasing the bandwidth as well as increasing the time delay have the same effect which is the extension of braking distance.

3-3-5 The Effect of Road Condition

In this project, the ABS uses only wheel speed sensors to detect our input variable wheel angular velocity, which can also be used to calculate reference slip ratio with estimated vehicle speed. Therefore, the road friction coefficient, which determines the vehicle deceleration during braking, is an important parameter to estimate vehicle speed. This section analyzes braking performances on different road surfaces and make an optimal tuning for each road surface.

The model here we used is:

$$\mu(\lambda; \theta_r) = \theta_{r1}[1 - exp(-\lambda\theta_{r2})] - \lambda\theta_{r3}$$

By changing the values of these three parameters, many different road conditions can be modeled. In Table 3-3, the corresponding parameters are listed. In this section these four curves will be used to study the effect of different road conditions.

First we keep the optimal tuning fixed, just change the surface to detect the effects, the results are shown in Figure 3-15

From Figure 3-15 we can see that by using optimal tuning parameters of asphalt dry in other road conditions, the work performances are not good. For asphalt wet surface,from Figure 3-15(b) we can see that at the beginning of the brake process, the wheel almost lock up. Because according to the road surface characteristic map, the value of $\mu(\lambda^*)$ of asphalt wet is much smaller than asphalt dry, if use the same u_1 in phase 1, the decrease torque derivative is not large enough, the wheel might lock up. For cobblestone surface, we can see that our algorithm works, but the problem is that the braking distance is longer than before due to the small value of $\mu(\lambda^*)$ by using the same tuning in asphalt dry surface. For snow surface, we can see that the wheel lock up quickly, since the maximum value of $\mu(\lambda^*)$ is really too small.

Now change the parameters to find the optimal setting for each condition. The initial brake speed is 130 km/h.

For wet asphalt road surface, after several tests, the optimized settings are $\epsilon_{1,5} = 30\ m/s^2, \epsilon_2 = 35\ m/s^2, \epsilon_{3,4} = 25\ m/^2$ and $u_1 = 2.1 \times 10^5\ pa, u_2 = 0, u_3 = 2 \times 10^4\ pa, u_4 =$

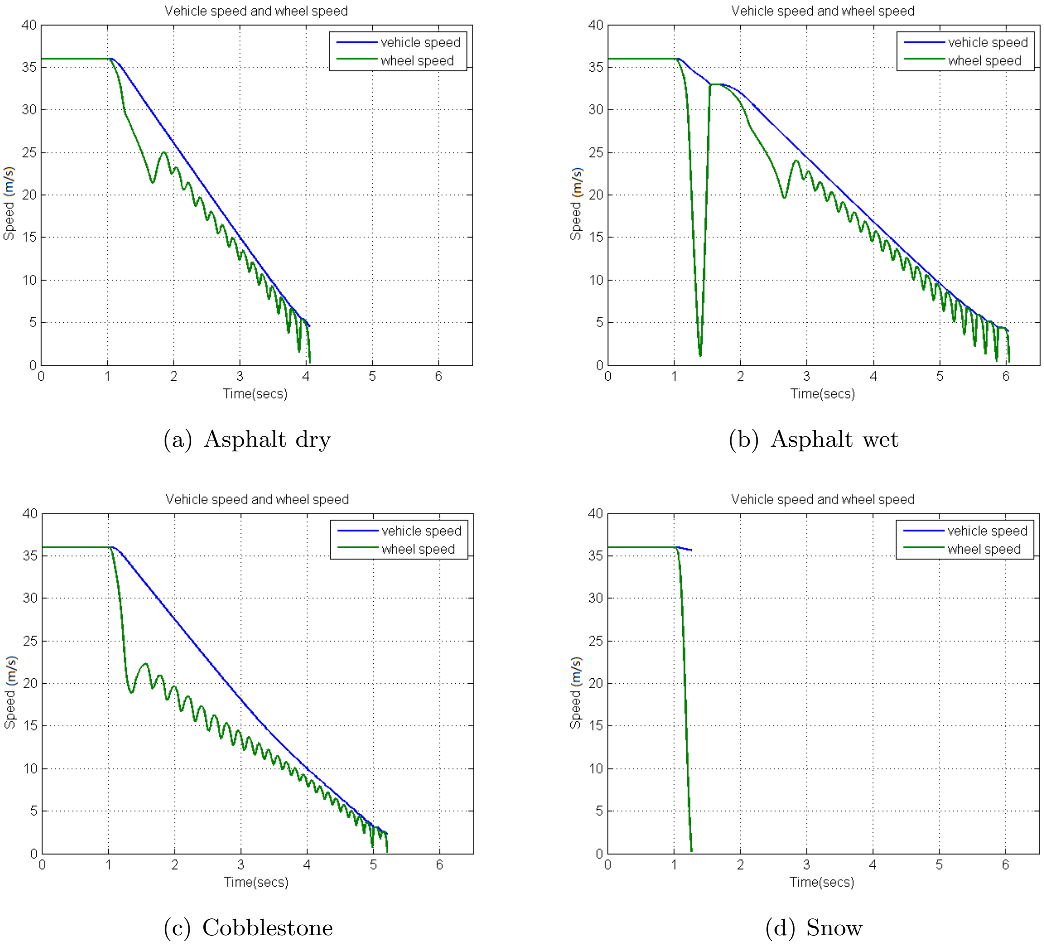

Figure 3-15: Fixed tuning with different road surfaces

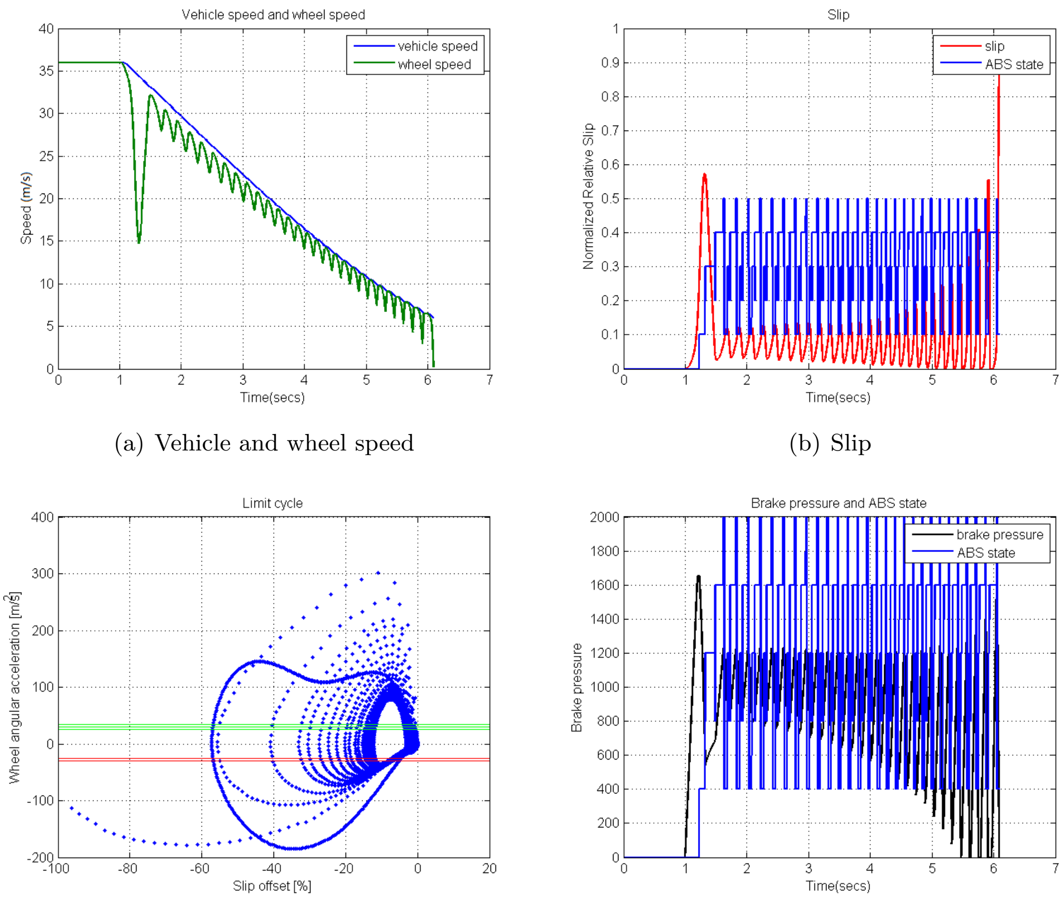

(a) Vehicle and wheel speed

(b) Slip

(c) Limit cycle

(d) Brake pressure

Figure 3-16: Optimal tuning for wet asphalt surface

$1.3 \times 10^5\ pa, u_5 = 220\ pa$. The results are shown in Figure 3-16, the braking distance is $d = 100.08\ m$ we can see that on the wet asphalt road condition, the braking distance is much longer than the dry asphalt due to the small value of $\mu(\lambda^*)$.

For cobblestone road surface, the optimized settings are $\epsilon_{1,5} = 30\ m/s^2, \epsilon_2 = 35\ m/s^2, \epsilon_{3,4} = 25\ m/^2$ and $u_1 = 6 \times 10^4\ pa, u_2 = 0, u_3 = 8.1 \times 10^3\ pa, u_4 = 8.2 \times 10^4\ pa, u_5 = 220\ pa$. The results are shown in Figure 3-17 and the braking distance $d = 71.58\ m$, clearly, the brake distance on the cobblestone road is shorter than the road of wet asphalt but still larger than the dry asphalt road surface, these differences can be well explained by the map of road-wheel coefficient of friction, the peak value of Asphalt dry is larger than the Cobblestone and Asphalt wet.

For snow road surface, the optimized settings are $\epsilon_{1,5} = 30\ m/s^2, \epsilon_2 = 35\ m/s^2, \epsilon_{3,4} = 25\ m/^2$ and $u_1 = 5 \times 10^5\ pa, u_2 = 0, u_3 = 2 \times 10^4\ pa, u_4 = 2 \times 10^5\ pa, u_5 = 220\ pa$. The braking distance is $d = 696.86\ m$.

After studying the optimal tuning on different road surfaces, the robustness analysis

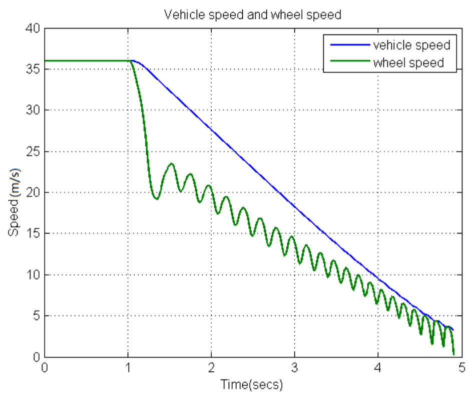

(a) Vehicle and wheel speed

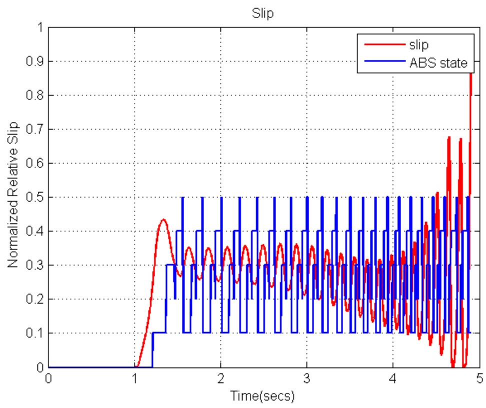

(b) Slip

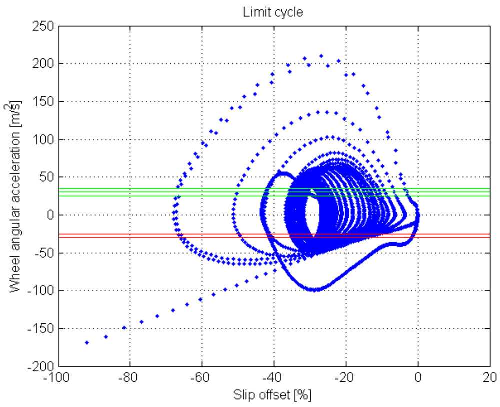

(c) Limit cycle

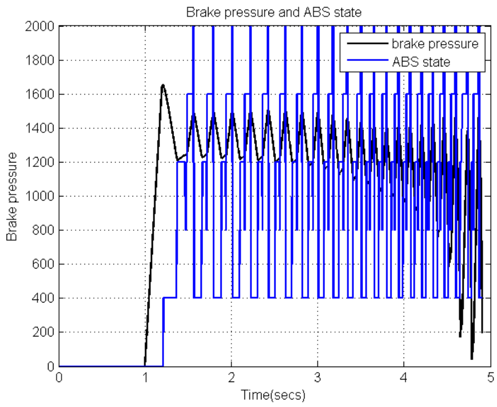

(d) Brake pressure

Figure 3-17: Optimal tuning for cobblestone surface

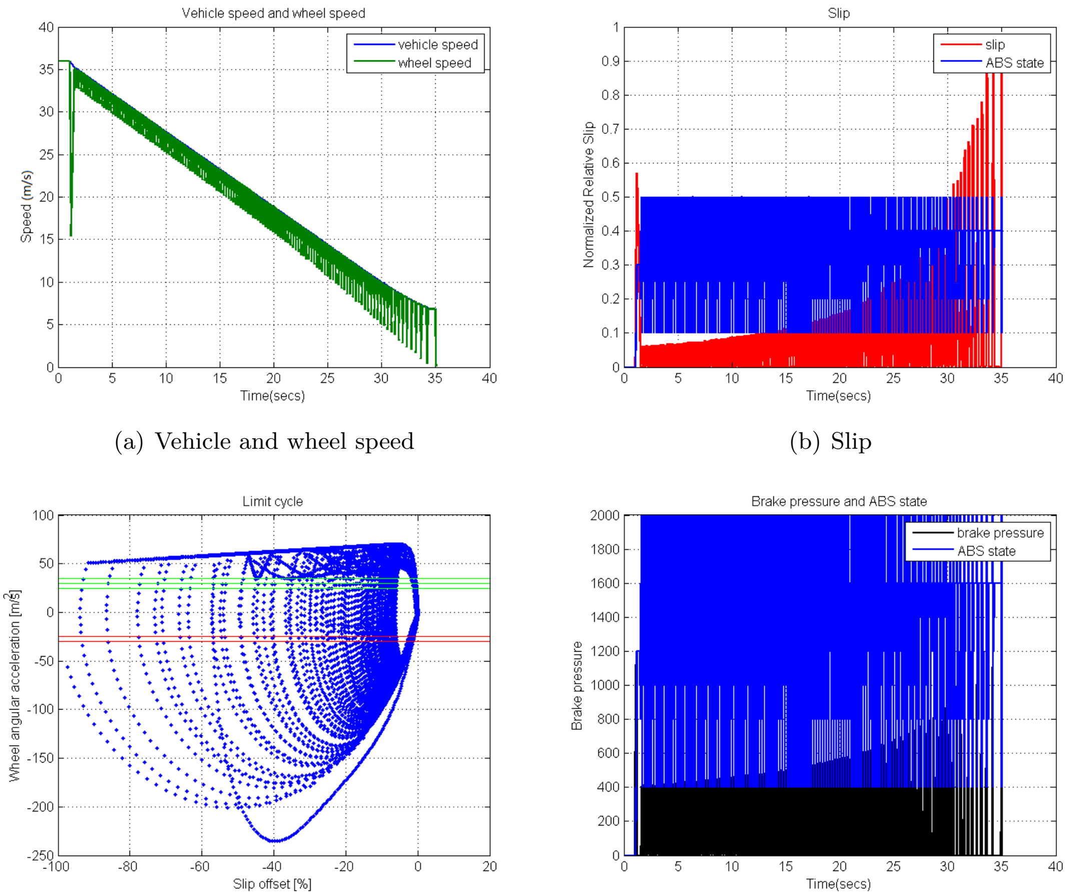

(a) Vehicle and wheel speed

(b) Slip

(c) Limit cycle

(d) Brake pressure

Figure 3-18: Optimal tuning for snow surface

Table 3-4: Braking distance ($4\ ms$ delay) for different additional inertia

Inertia	Braking distance
$2.6063\ kg \cdot m^2$	$\int_{v_0}^{7} vdt = 59.51\ m$
$3.8563\ kg \cdot m^2$	$\int_{v_0}^{7} vdt = 59.55\ m$
$5.1063\ kg \cdot m^2$	$\int_{v_0}^{7} vdt = 59.55\ m$

also need to be considered. We hope we can find one optimal tuning for all different road conditions, actually during this project, by testing on different road surfaces, it is really difficult to find an optimal tuning that could be implemented for snow and asphalt dry road surface (from the road surface characteristic map in chapter 2, we can see their peak values are really different). For example, in phase 1, if we use a large pressure derivative, this could prevent the wheel from locking up on the snow surface. However, according to the previous sensitivity analysis, this value is really large for asphalt dry road surface (maybe lead to a long braking distance). In another side, if the pressure derivative is not large enough which is reasonable for asphalt dry, but when apply to the snow surface, it maybe will lead the wheel lock up.

The difference between the asphalt dry and the cobblestone is not big, it is possible to find one optimal tuning that could adopted by such road conditions. This also convinced by the values of optimal tuning on these two road conditions.

3-3-6 The Effect of Inertia

In this thesis, we will use an electric motor, since we introduce an electric motor to our brake system, so the inertia changes. Actually, in this project, the inertia of the motor we used is $0.036\ kg \cdot m^2$. In this section, we test the additional inertia sensitivity, here we use three different additional inertia values, $0.225\ kg \cdot m^2, 0.425\ kg \cdot m^2, 0.625\ kg \cdot m^2$. According to the transmission section analysis, we know that by transmitting to the wheel side, the equivalent inertia should be equal to $i^2 \cdot J$, so the values of inertia on the wheel side are . The results are shown in Table 3-4. From the results we can see that the braking distance is not so sensitive to the additional inertia changed.

3-4 Short Conclusion

This chapter presents one of traditional control approaches that is wheel deceleration control. In this thesis project we use five phase algorithm control strategy in our system. In this algorithm, there are two variables, the deceleration threshold ϵ and the pressure derivative u, based on the sensitivity analysis, the optimal tuning for the asphalt dry road condition is found. And the effects of transport time delay, bandwidth, inertia changed and road surface are introduced separately. Based on the optimal tuning found in this chapter, the following chapter will study the regenerative braking, the electric motor will corporate work with the friction brake.

The control of ABS is complicated and sometimes may not be effective due to the non-linear characteristics and unknown environmental parameters. In the modern vehicle design many control algorithms are proposed such as fuzzy logic control [20][21][22], neural network [23], and other intelligent control [24][25][26].

Chapter 4

Regenerative Brake Control

In conventional brake designs, the forward momentum of the vehicle is lost when the brakes are applied. This energy is converted to heat via friction and is dissipated into the surrounding air. In order to reuse this lost energy, the regenerative braking is come to light.

The regenerative braking enables the vehicle to capture some of the energy that would otherwise be lost when the vehicle slows to a stop. The applied braking force is proportional to the current ($T_m = K_t \cdot I$). The regenerative braking process slows the vehicle but not enough to bring the car to a stop exactly. Generally, a regenerative braking system is typically used in parallel with a traditional friction brake design, the reasons are: (1) the regenerative braking torque is not large enough to cover the required braking torque; (2) the regenerative braking can not be used for many reasons such as a high state of charge (SOC) or high temperature of the battery to increase the battery life [27].

Having two brake systems sounds like a good idea from a safety perspective, but it also means that the actions of these two independent systems need to be coordinated to balance energy recovery with the need for braking precision.

According to the actions of two braking systems, we know that the hydraulic brake does not react fast enough to provide precise braking controls due to the time delay. Electric motor brakes have fast dynamics response but the torque is limited. So in the coming up sections we will study how to combine them together and improve the braking performance.

4-1 Friction and Motor Brake Cooperative Work without ABS

First we disconnect our ABS controller, then we make a torque allocation of the motor brake and friction brake.

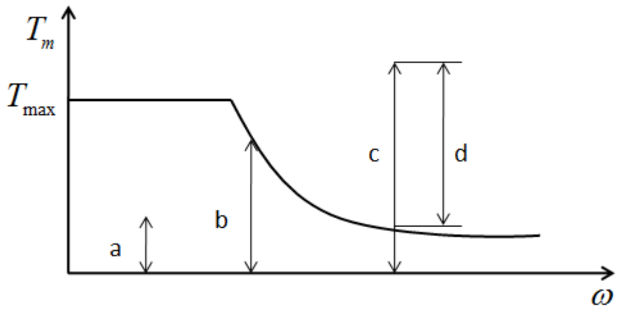

Figure 4-1: Motor torque characteristics

In order to provide an appropriate motor brake torque for a given driving condition, a control algorithm is required to determine the allocation of the motor brake and friction brake corresponding to the driver's demand. Figure 4-1 shows the motor characteristic curve used in this design.

From Figure 4-1 we can see that. If the required motor torque is a, the braking can be achieved only by the motor brake since a is smaller than the available motor torque. When a braking torque c which is larger than the available motor torque is demanded, the conventional friction brake has to be operated together with motor braking to supply the missing torque, d. Also the motor power limitation need to be taken into account. Thus the algorithm we used in this design can be presented in Figure 4-2:

Now using the control structure depicted in Figure 4-3 to test the system performance, in this structure we can see we have three input variables which are driver desired brake torque $T_{desired}$, wheel speed ω and estimated friction brake efficiency $\hat{\gamma}$. The outputs are motor current I and pressure P which can be calculated by using equations $I = T_{motorreal}/K_t$ and $P = T_{friction}/\hat{\gamma}$ respectively. Since we know that the parameter γ depends on the brake temperature and is difficult to model. During this design we use $\hat{\gamma}$ to estimate it. The specifications of motor are listed in Table 4-1. The testing results are shown in Figure 4-4.

Figure 4-4(a) and Figure 4-4(b) show the results of different brake torques, we can see that for a larger torque, the controller works in the condition $T_{desired}\omega > P_{max}$, so the brake system calls for additional friction brake torque. Notice that in the motor torque curve there are two kick points, the first one is due to the motor max power limit which is equal to P_{max}/ω, and another point is due to the motor max torque limit which is saturated by T_{max}. For a smaller torque, it works in the condition $T_{desire}\omega < P_{max}$, so the motor can supply the whole brake torque.

Figure 4-4(c) and Figure 4-4(d) represent the results of different initial speeds. For speed 20 m/s, the power limited torque is larger than the max motor torque limited, so we can see the motor torque first increases linearly then keep constant due to the max torque limited.

Figure 4-4(e) and Figure 4-4(f) represent the effects of $\hat{\gamma}$. In the actuator part we already introduced this parameter which is difficult to model, in this project we just

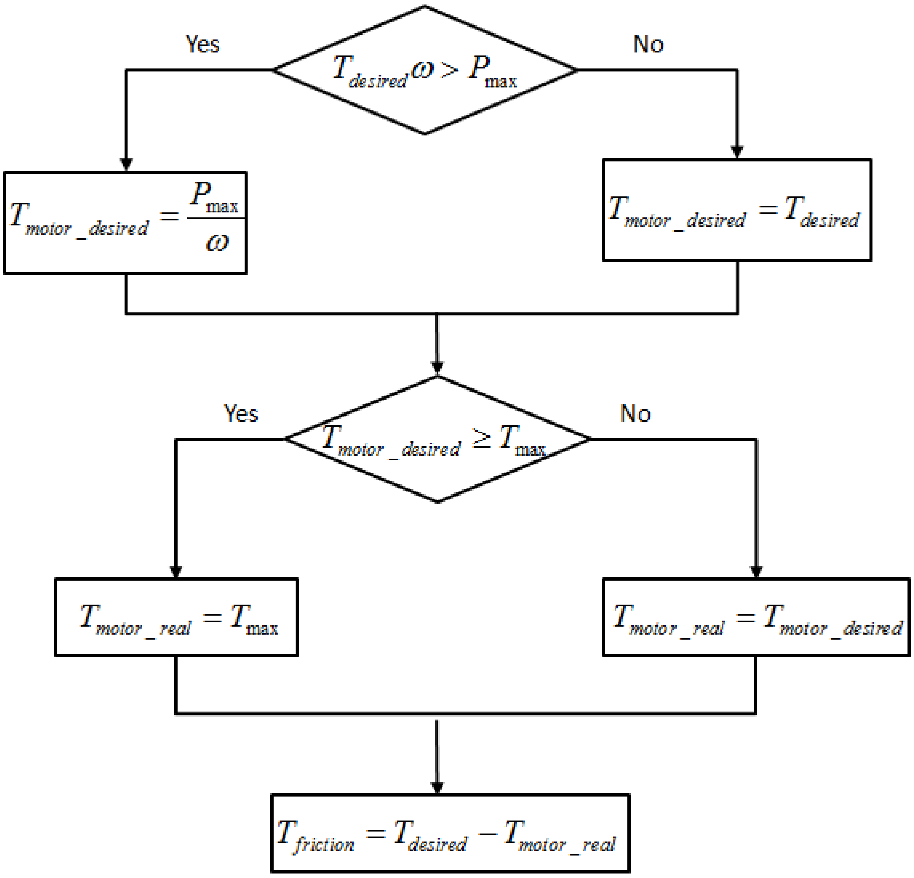

Figure 4-2: Brake torque allocation flow chart

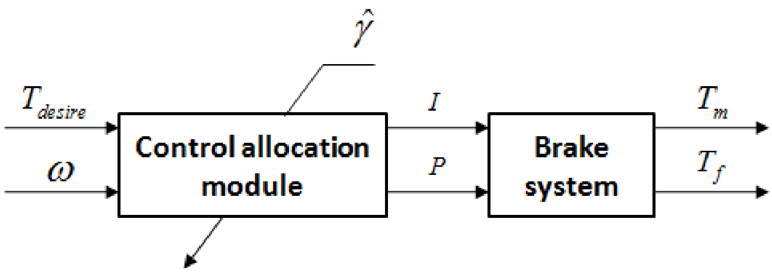

Figure 4-3: Brake system with control allocation module

Table 4-1: Motor specification

Item	Symbol	Value	Units
Max power	P_{max}	56280	w
Inertia	J_m	0.036	$kg \cdot m^2$
Resistance	R_{in}	0.056	Ohm
Inductance	L	0.00213	H
Max current	I_{max}	329	A
EMF constant	K_e	1.37	Vs
Torque constant	K_t	2.37	Nm/A
Max torque	T_{max}	286	Nm

assume that $\hat{\gamma} = \gamma$, but here we have a quick sight to check its effect. We know the control variable pressure can be computed from $P = T_{friction}/\hat{\gamma}$, if the estimated value of $\hat{\gamma}$ is larger than the real value of γ, from the equation, we know the value of P will become small then the friction brake torque will decrease, this can be seen from Figure 4-4(e). The actual brake torque is smaller than the desired brake torque (which would increase the braking distance). If $\hat{\gamma} < \gamma$, the actual brake torque is larger than the desired torque (which would lead to the wheel lock up). In this project, the more interesting thing is to study the performance of friction and motor brake, also due to the time constraint, this variable is not controlled, we can just briefly assume that $\hat{\gamma} = \gamma$.

Now we change the road surface to test the controller performance. The initial parameters setting here are: $T_{desired} = 1500\ Nm, v_0 = 36\ m/s, \hat{\gamma} = \gamma$. The results are shown in Figure 4-5. Obviously, the performances are different due to the different road conditions, but from these figures we can see that the motor brake torque with friction brake torque is equal to the desired brake torque, our control allocation module works well. In the following section, we will implement the ABS controller into the brake system.

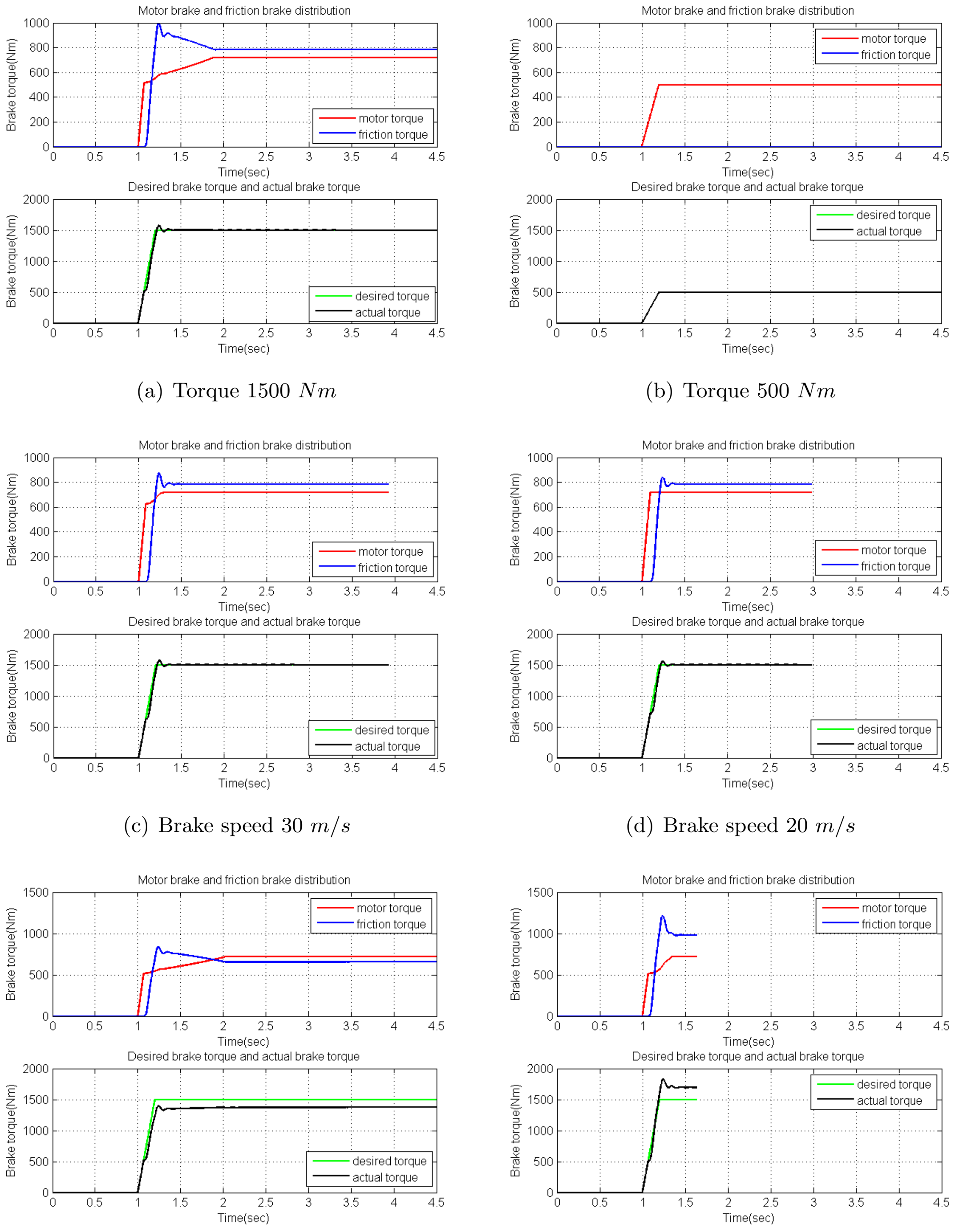

(a) Torque 1500 Nm

(b) Torque 500 Nm

(c) Brake speed 30 m/s

(d) Brake speed 20 m/s

(e) $\hat{\gamma} > \gamma$

(f) $\hat{\gamma} < \gamma$

Figure 4-4: Input variables of control allocation module test

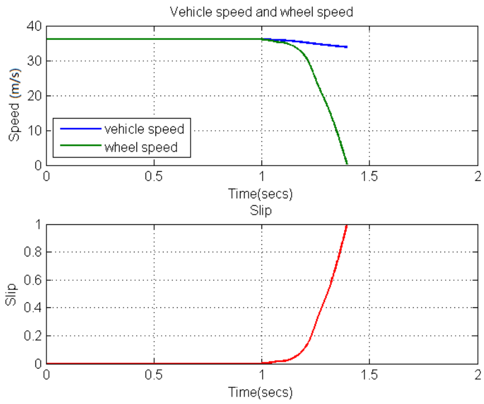

(a) Asphalt wet: speed

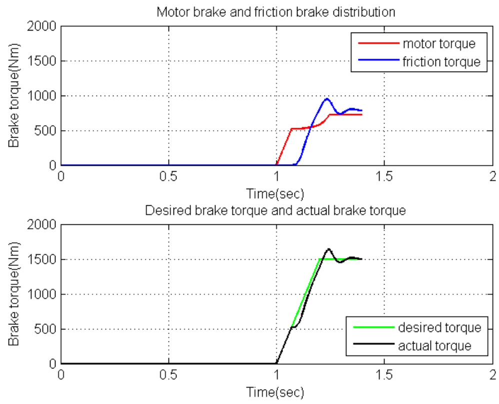

(b) Asphalt wet: torque

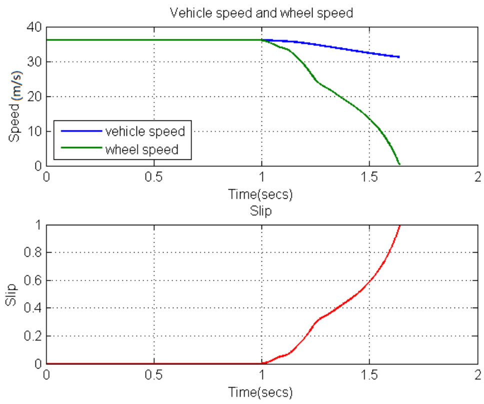

(c) Cobblestone: speed

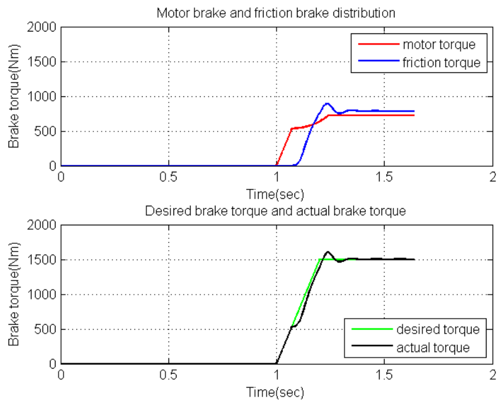

(d) Cobblestone: torque

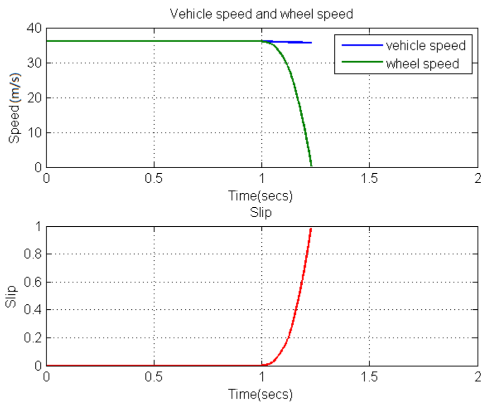

(e) Snow: speed

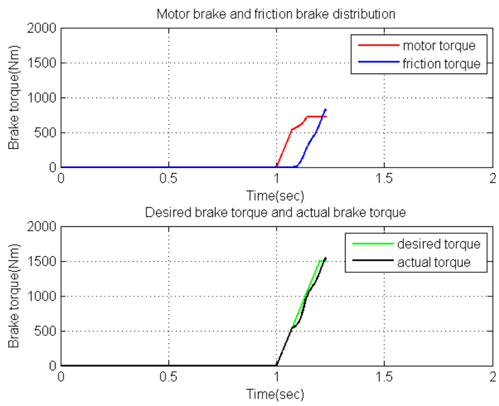

(f) Snow: torque

Figure 4-5: Control allocation module test with different road conditions

4-2 Friction and Motor Brake Cooperative Work Equipped with ABS

In the previous section, we already designed a control allocation controller. Now we need to implement the ABS controller to the brake system, the system structure is presented in Figure 4-6.

First, we just keep the optimal tuning which is presented in the last chapter fixed, and check the results. In another word, we add a motor brake model and a distribute controller to the traditional friction brake structure. Now we have to consider two things, the first one is braking distance what we want to minimize, the second thing is the recovered energy what we want to maximize. During this design, we study the performance of torque coordinate work for the high speed region (from initial speed to $7\ m/s$). The initial parameters setting here are: $T_{desired} = 1650\ Nm, v_0 = 36\ m/s, \hat{\gamma} = \gamma$. The torque allocation is shown in Figure 4-7(a).

Braking distance is:

$$d = \int_{v_0}^{7} vdt = 60.28\ m$$

Recovered energy is:

$$E = \int Pdt = 60\ kJ$$

Compare to the traditional friction brake in the last chapter, the braking distance is $60.48\ m$, we can see it is improved. Because motor brake has fast dynamics response, there is no time delay, so once the desired brake torque signal is implemented, the motor will generate the brake torque immediately.

As introduced in chapter 2, the friction brake has slow dynamics and the motor brake has fast dynamics. The control allocation module we used in Figure 4-6 finally we can see that motor torque is constant due to the torque limited and the friction brake vibrates by increasing or decreasing the hydraulic pressure according to the ABS control algorithm.

However, the hydraulic system has a time delay, the response control action is a little bit late, and the electric motor has fast dynamics, no time delay. Thus, we want to take advantage of this property, so we make the friction brake torque constant and ABS will work on the motor torque by controlling the current. The torque allocation is shown in Figure 4-7(b). In order to compare with the previous regenerative brake, we compute the braking distance and recovered energy again.

Braking distance is:

$$d = \int_{v_0}^{7} vdt = 58.97\ m$$

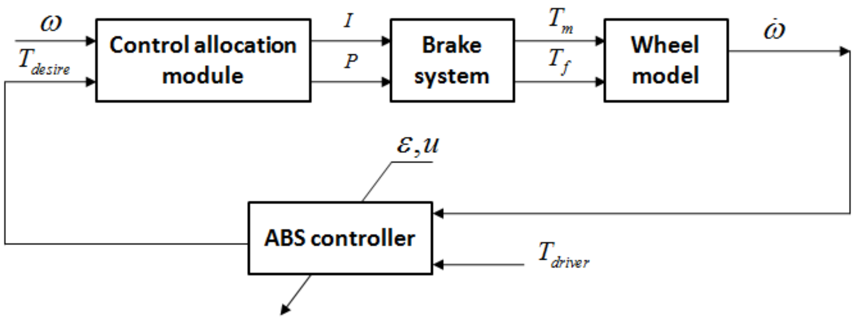

Figure 4-6: Friction and motor brake cooperative work equipped with ABS

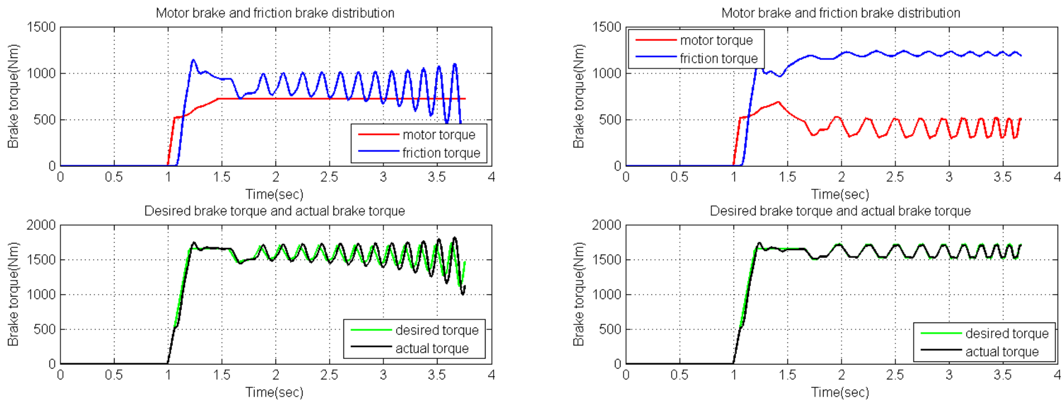

(a) Motor torque constant (b) Friction torque constant

Figure 4-7: Two different cases. The first figure is motor torque constant, finally works at the maximum motor torque, the recovered energy is maximum. The second figure is friction constant, due to the motor fast dynamics, the braking distance should be shorter than the first case, but the recovered energy is lower.

Table 4-2: Brake performance comparison

System	Torque distribution	Braking distance	Recovered energy
1st structure	friction brake vibrate	60.28 m	60 kJ
2nd structure	motor brake vibrate	58.97 m	39.60 kJ

Recovered energy is:

$$E = \int P dt = 39.60 \ kJ$$

The comparison of the results in these two structures are listed in Table 4-2. Clearly, in the first structure the motor torque is constant at max torque, compare to the second structure the recovered energy is much larger, but the braking distance is longer than the second structure. In the first case, the ABS algorithm works on the friction brake, due to the time delay of friction brake, the braking distance becomes longer (1.31 m). However, in the opposite case, in the second structure, we keep friction constant, the ABS algorithm works on the motor brake (no time delay), the braking distance improved. However, the recovered energy is less than before, the recovered energy of the 2nd case is only 66% of the 1st case.

Notice that, the purpose here is to show two really different conditions, because we have two cost functions, in the first case we can see we got much more recovered energy, but the braking distance is longer. In the second case, the braking distance is improved, but the recovered energy is really smaller than the first case.

In Figure 4-8 we draw a map for these two functions, the x axis stands for the recovered energy, the y axis is represented by the braking distance. The red dot lines shown in Figure 4-8 depict the minimum braking distance and the maximum recovered energy respectively. From the road surface map we can easily find the maximum of the brake force, so the minimum braking distance can be easily calculated by using this value, and the maximum recovered energy limited by the electric motor power. Also the results of the previous two cases are plotted in the figure.

Obviously, the cross point of these two lines is the best performance, but actually according to the previous analysis, it is really impossible to reach to this point, the trade off must be made. For example, in case 1, if we can keep this recovered energy and decrease the braking distance, or in case 2, if we can keep the braking distance and increase the recovered energy, or if there is some other approaches to make a trade off. So the coming up work also the goal of this project is to find the trade off between the braking distance and the recovered energy.

4-3 Frequency Splitter

From the last section we already tested two different structures (motor torque constant and friction torque constant separately), now the more interesting thing as shown in

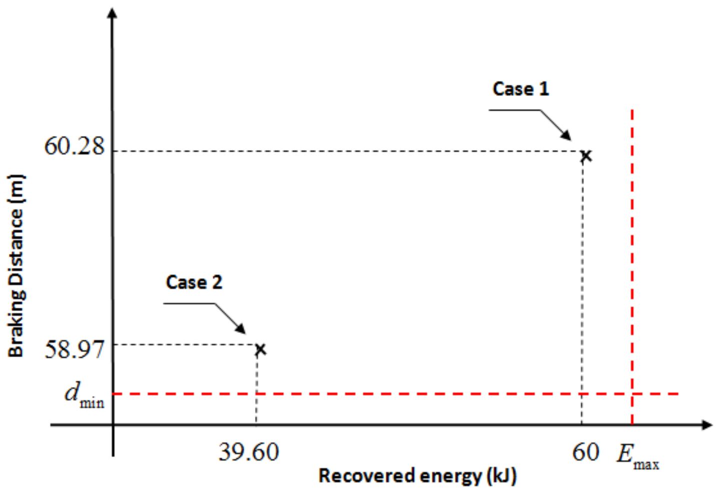

Figure 4-8: Trade off between the braking distance and the recovered energy

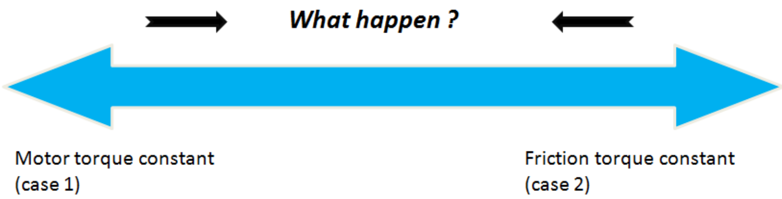

Figure 4-9: Change direction

Figure 4-9 is that what will happen if we make a trade off. According to the characteristics of friction and motor brake, we know that the friction brake has time delay but the brake torque is large, motor brake has fast dynamics but the max torque is not big enough. So in order to take advantage of their properties, we put a low pass filter (see Figure 4-10) into the control allocation module. By choosing a cut-off frequency F_c, the low frequency part applies to the friction brake, and the high frequency part applies to the motor brake. Now the whole system model is shown in Figure 4-11.

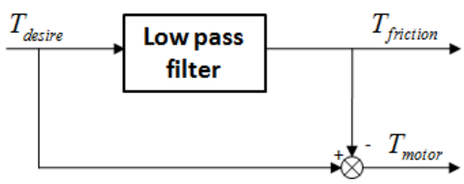

Figure 4-10: Low pass filter module

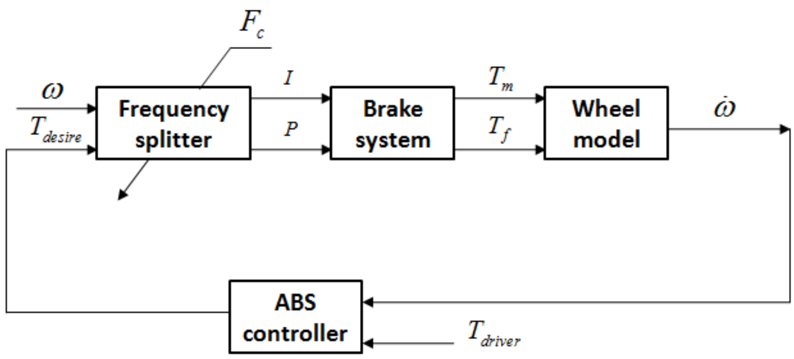

Figure 4-11: Final brake model

4-3-1 Frequency Splitter Analysis

Here we test our frequency splitter by using a signal that contains both low frequency and high frequency, the input sinusoidal signal contains low frequency part (0.15 Hz) and high frequency part (79.57 Hz). After going through the splitter, the results are shown in Figure 4-12. As we can see, if the cut-off frequency is really small, the low frequency part almost equal to zero, and the whole signal will pass through the high frequency, because according to our structure, we use the total input signal minus the frequency part to get the high frequency part, now the low frequency part is zero, so the total input signal will pass through the high frequency part. If the cut-off frequency is too big, the whole input signal will pass through the low frequency part, so the high frequency part will be zero.

4-3-2 Constant ABS tuning

As we introduced before, our global objective is to test the performance of the system by considering two factors (braking distance d and recovered energy E). From our final model we can see that in this model there are three parameters, for ABS controller we have two parameters which are deceleration threshold ϵ and pressure derivative u, for frequency splitter we have one parameter which is cut-off frequency F_c.

Actually the tuning of ABS is done empirically, design a new ABS controller is really expensive in term of time, also it is not the goal in this project. Therefore, we use a constant ABS parameters $\bar{\epsilon}, \bar{u}$ and just tuning the cut-off frequency F_c. So the coming up work is to decide the constant ABS parameters $\bar{\epsilon}, \bar{u}$.

Our hybrid brake model has two brake modules, the hydraulic module has time delay 7 ms and the electric motor brake module has 0 ms time delay. From the left plot of Figure 4-13, we can see, after going through the controller, our desired torque is separated into two parts, one is applied to the hydraulic brake and another one is applied on the motor brake then we get our final actual brake torque with a time delay. Clearly, if the brake torque allocation is different, the delay of this hybrid system is different, so this variable is changing. In order to tune $\bar{\epsilon}, \bar{u}$ we want to use a unique

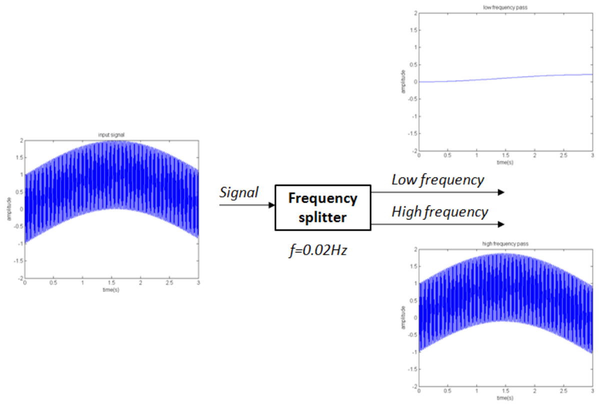

(a) Cut-off frequency $f = 0.02\ Hz$. The cut-off frequency is very small, thus low pass filter loses split ability, the low frequency shown in figure almost equal to zero.

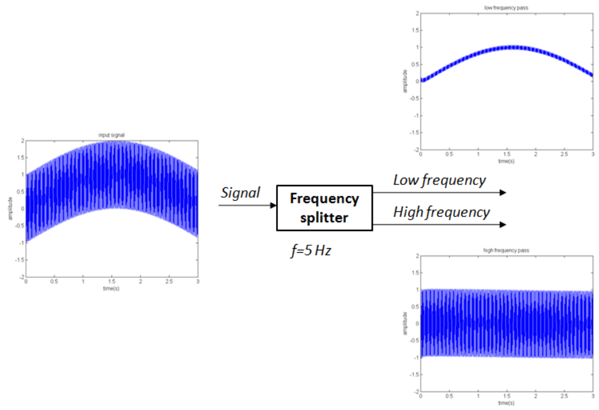

(b) Cut-off frequency $f = 5\ Hz$. The signal separate into two parts (low frequency and high frequency) what we expected.

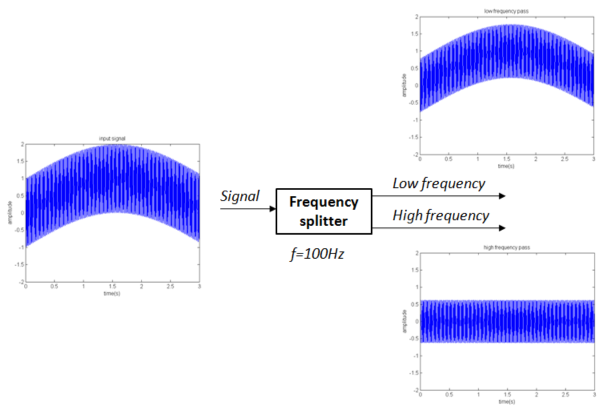

(c) Cut-off frequency $f = 100\ Hz$. Since the cut-off frequency is really large, the whole signal pass through low frequency part, and the high frequency part almost equal to zero.

Figure 4-12: Signal test: low frequency vs high frequency

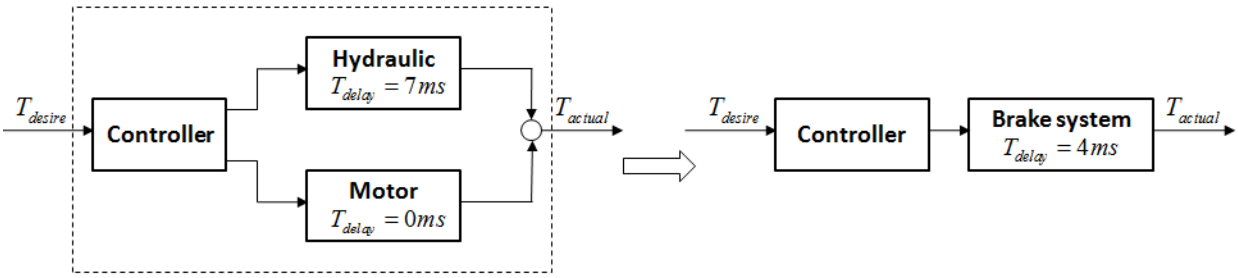

Figure 4-13: Time delay module

Table 4-3: Braking distance (additional inertia) for different time delay

Delay	Braking distance
$7\ ms$	$\int_{v_0}^{7} vdt = 60.38\ m$
$4\ ms$	$\int_{v_0}^{7} vdt = 60.24\ m$
$2\ ms$	$\int_{v_0}^{7} vdt = 60.12\ m$

time delay, also the ABS controller should work for the whole system, thus we choose an average time delay as 4 ms, this can be seen in the right plot of Figure 4-13.

Since we introduce a electric motor to our brake system, so the system inertia changes. As introduced in chapter 2, here we add this equivalent motor inertia change on wheel side, the value is $J_m \cdot i^2$. The structure for this testing we used is the traditional friction brake with ABS, the only thing we need to change is wheel side inertia now we use $J_w + J_m \cdot i^2$. Using the previous fixed optimal tuning we test three different time delay $7\ ms, 4\ ms, 2\ ms$ respectively. The results are shown in Table 4-3.

Clearly, along with the time delay decreasing, the braking distance is decreasing, the reason is already explained in last chapter. Now we make an optimal tuning for the average time delay 4 ms, after tuning and testing many times, the optimal values we selected are $\epsilon_1 = 23, \epsilon_2 = 30, \epsilon_3 = 20; u_1 = 4.8 \times 10^4, u_3 = 3.5 \times 10^4, u_4 = 5 \times 10^4, u_5 = 220$. The braking distance is:

$$d = \int_{v_0}^{7} vdt = 59.51\ m$$

4-3-3 Improved Schematic with Frequency Splitter

Now we implement this constant ABS setting to our final model, then we start to check the sensitivity for the cut-off frequency F_c, first we choose a value 4 Hz, the brake torque allocation plot is shown in Figure 4-14. From this figure we can see that the motor brake torque vibrates around zero, so it is not good for improving the braking performance, we hope motor brake can play a more important role. So we introduce a new bias parameter to boost this average level.

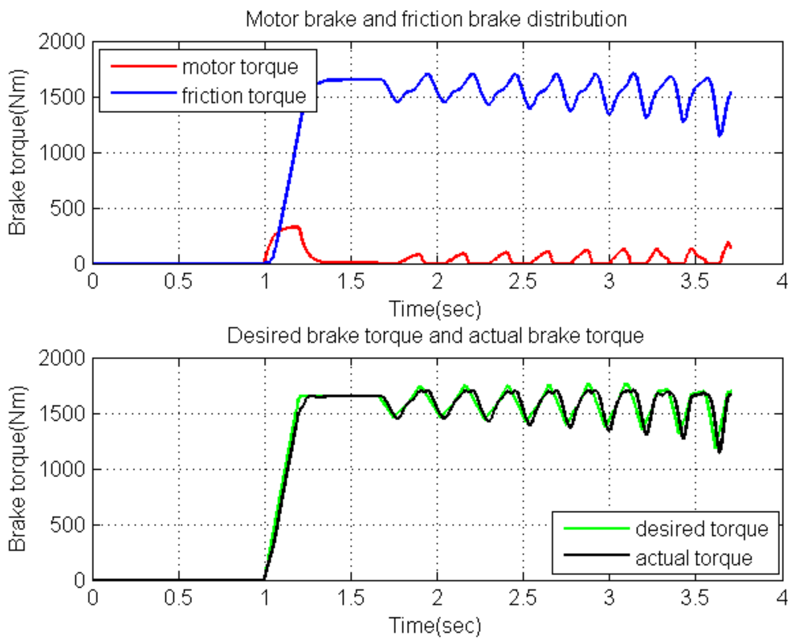

Figure 4-14: Brake torque allocation

The sensitivity testing results of the cut-off frequency is shown in Figure 4-15. By calling back the previous explanation of signal test Figure 4-12(a), if the cut-off frequency is very small, thus low pass filter loses split ability, the low frequency shown in the figure almost equal to zero. From Figure 4-15(a) we can see that the motor torque works at the maximum torque due to the torque limitation, but the total brake torque is larger than it, so still we need friction brake torque.

However, If the cut-off frequency is very big, from the previous explanation of signal test Figure 4-12(c), we know the whole signal pass through low frequency part, and the high frequency part almost equal to zero. Here we can see the motor torque is not equal to zero, because we already used a bias value 400 Nm, so the motor torque here is equal to 400 Nm, this can be seen in Figure 4-15(f). Clearly, the motor bias value will effect our braking performance, this parameter must be taken into account in this design.

By using a vector of frequency values (from 1.5 Hz to 15 Hz), we test the effects of different motor bias constant value, here we use 300 Nm, 500 Nm, 700 Nm, the results are shown in Figure 4-16.

From this figure we can see that by increasing the bias constant value, the braking distance is decreasing and the recovered energy is increasing, but when this value closes to the maximum of motor torque (for example, when bias value equals to 700 Nm), the braking distance is increasing (see black line in Figure 4-16). The explanation for this situation can be represented in Figure 4-17, since the value is large, so we can see it exceeds the maximum motor torque, and the actual motor brake torque is saturated by this maximum value, thus the braking performance is restricted.

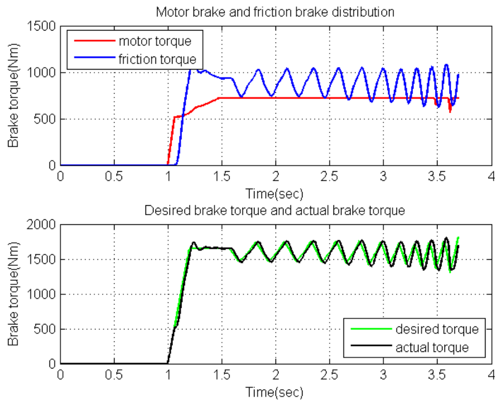

(a) cut-off frequency: 0.08 Hz

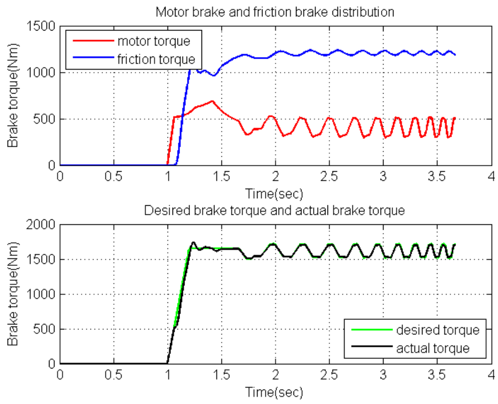

(b) cut-off frequency: 0.9 Hz

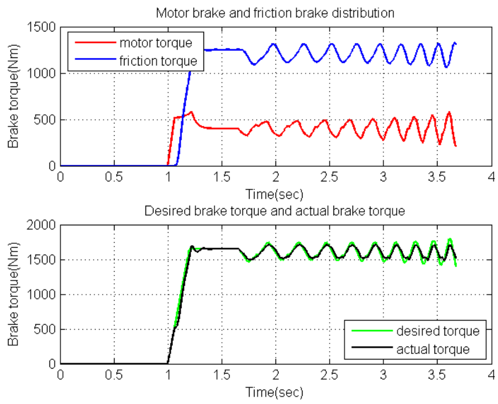

(c) cut-off frequency: 4 Hz

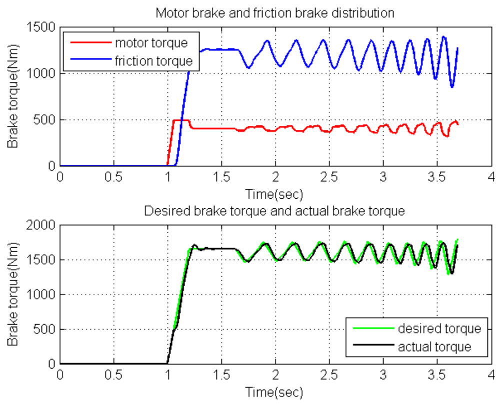

(d) cut-off frequency: 15 Hz

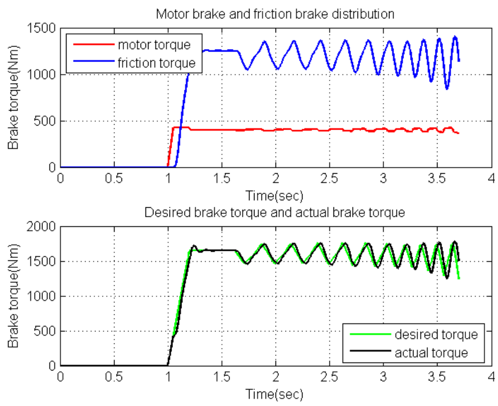

(e) cut-off frequency: 50 Hz

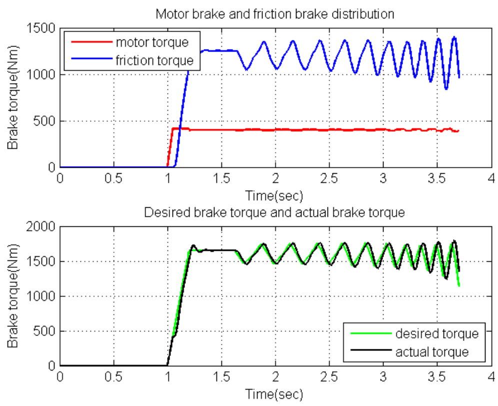

(f) cut-off frequency: 100 Hz

Figure 4-15: Torque allocation with different cut-off frequency

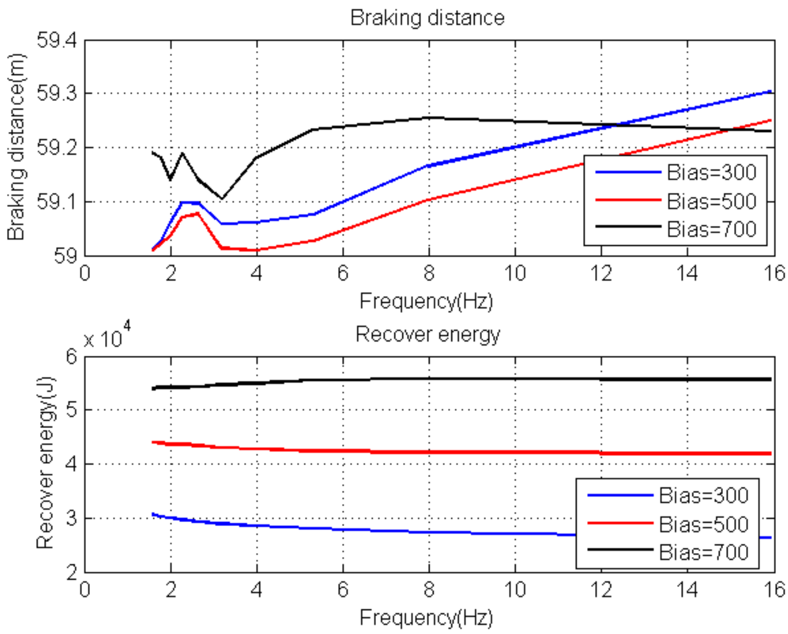

Figure 4-16: Brake performance with different constant bias values

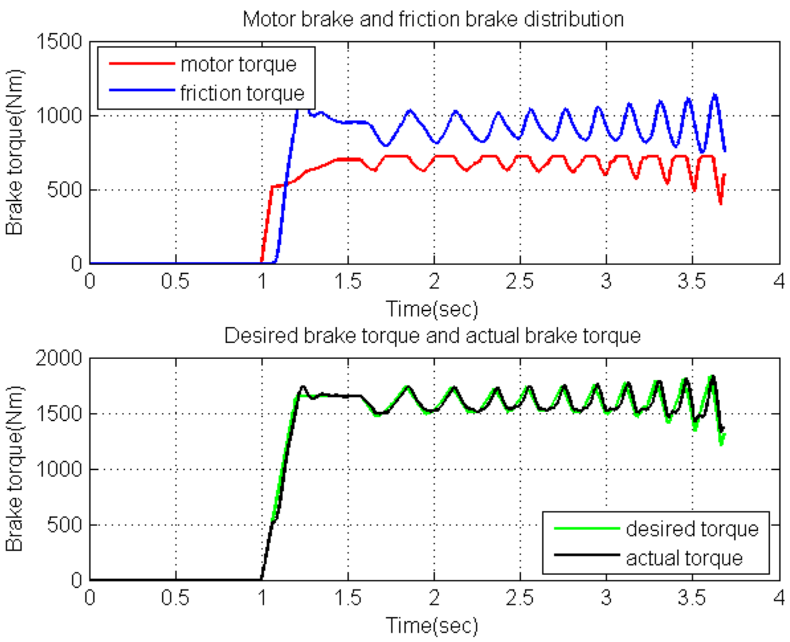

Figure 4-17: Brake performance with large constant bias value

Until now we already analysis the sensitivity of the cut-off frequency and the motor bias parameter, in order to find a more accurately boundary shape, now we use couple of the motor bias values and the cut-off frequencies to find the cost function boundary, the results are shown in Figure 4-18(a). By using these results we can draw our cost function boundary, the shape is shown in Figure 4-18(b).

4-4 Short Conclusion

In the regenerative braking, two actuators (friction brake and motor brake)need to be merged and two cost functions need to be made a trade off. First we consider two different cases by setting motor torque constant and friction torque constant separately. By implementing a low pass filter we can distribute brake torque, low frequency region will apply to the friction brake, and high frequency region will implement to the motor brake. After tuning the cut-off frequency of low pass filter, a series of data depicted a boundary between braking distance and recovered energy what we expect to get.

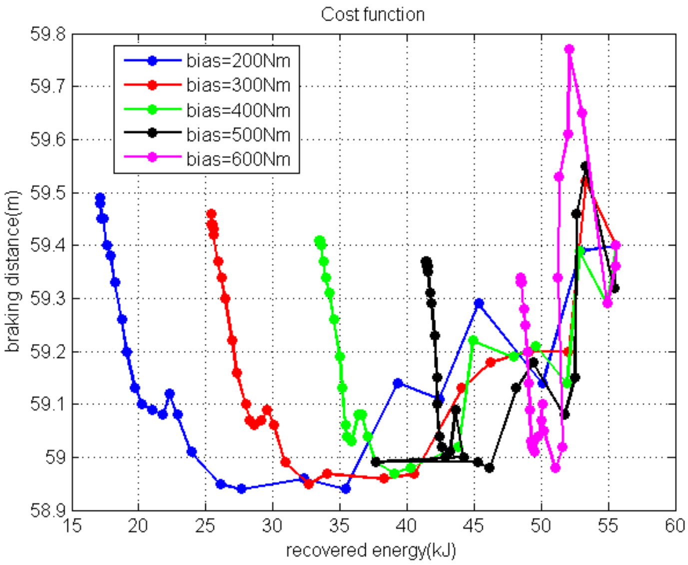

(a) Test results of different cut-off frequency and motor bias value

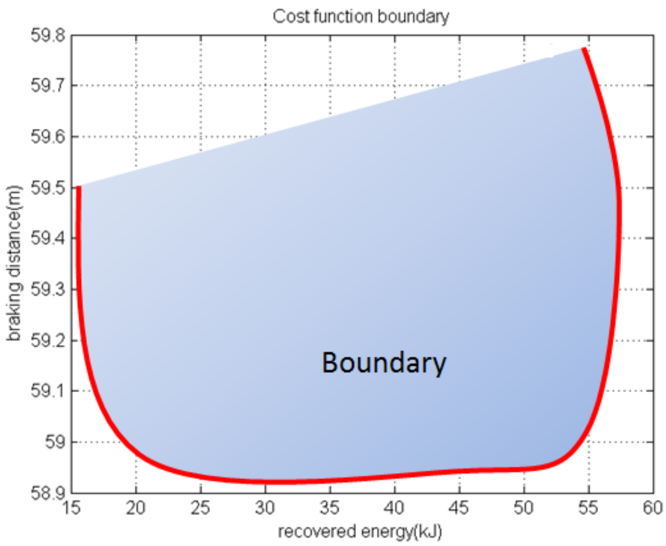

(b) Boundary shape

Figure 4-18: Cost function boundary

Chapter 5

Conclusions and Recommendation

5-1 Conclusions

This thesis report has been set out to accomplish the following goals:

1. Introduce the reader to nonlinear wheel dynamics and related brake control problems.
2. Describe two brake actuators, traditional hydraulic brake and electric motor brake.
3. Introduce a ABS wheel deceleration control based on the thresholds switching.
4. Present a model of the traditional friction brake system equipped with ABS and validate this model.
5. Present a model of the entire system (merge two actuators)and test this model.
6. Verify the developed controller performance by considering the braking distance and recovered energy.

Based on the five phase algorithm used in traditional ABS control, we add a fast dynamics component electric motor to the system. The control problem in wheel deceleration control caused by the additional inertia changed in regenerative brake has been explained. By using a low pass filter, the friction brake torque and motor torque are distributed separately, the steps have been explained to understand the reasoning behind each area of the developed frequency splitter. The simulation programme of the entire system has been described in detail and validated using three structures. The boundary between braking distance and recovered energy has been found. Conclusions are that according to this project, the performance of braking distance is improved. However, in regenerative brake the braking distance and the recovered energy we need to make a trade off.

5-2 Recommendation

The thesis here seems to be an end but is really a new beginning, according to the whole process during this project, here I will list some recommendations

Road Surface In this project, the ABS uses only wheel speed sensors to detect the input variable wheel angular speed, which can also be used to calculate reference slip ratio with estimated vehicle speed. Therefore, the road friction coefficient, which determines the vehicle deceleration during braking, is an important parameter in estimation vehicle speed. In the chapter 3, the effect of road condition is done, the model we used is:

$$\mu(\lambda;\theta_r) = \theta_{r1}[1 - exp(-\lambda\theta_{r2})] - \lambda\theta_{r3}$$

By changing the value of θ_{ri}, many different road conditions can be modeled.

However, in the final part (regenerative braking equipped with ABS) due to the time limitation, we only got simulation tests on asphalt dry road surface. So future work should include the testing of the controller on other road surfaces such as asphalt wet or cobblestone surface.

Tire Test Bench In this thesis, all the results we obtained are simulated in the computer. In simulations, many controllers show robust behavior when tested in simulations and can cope with the nonlinearities described in Chapter 2. Nevertheless, a controller's performance is better observed by testing it on a real system. A controller's sensitivity to predefined noise signals or errors can be simulated, but the various influences on signals on an experimental setup such as drift, additive noise, delays, and other system dynamics make it a more thorough test. So, in future work, the control algorithms and the simulations what we have done in this thesis should be tested on a real tire test bench and implemented in a test vehicle.

Transmission The transmission gear implemented in the simulation is a reasonable constant value in order to simplified the model. For future work, a continuously variable transmission (CVT) is recommended. CVT is an emerging automotive transmission technology that offers a continuum of gear ratios between high and low extremes with fewer moving parts. In paper [4], CVT speed ratio control algorithm is suggested during the braking. The optimal operation line is obtained to operate the motor in the most efficient region. It is found from the simulation that the regenerative braking algorithm including the CVT ratio control provides improved fuel economy as much as 4 percent for federal urban driving schedule.

Friction Brake Coefficient In chapter 2 we already introduced this parameter γ which is friction brake coefficient, since it is a time varying variable, depends on the temperature, it is difficult to model. In this project we just assume that $\hat{\gamma} = \gamma$, but actually the estimation precision should be taken into account.

We know the control variable pressure can be computed from $P = T_{friction}/\hat{\gamma}$, and the friction brake torque expression is $T_f = \gamma \cdot P$, so we can see if the estimated value of

$\hat{\gamma}$ is larger than the real value of γ, the value of P will become small then the friction brake torque will decrease. In another side, if $\hat{\gamma} < \gamma$, the actual brake torque is larger than the desired torque.

Notice that, if our system is an open loop control, obviously, these estimate errors will effect our braking performance directly. However, our ABS system is a closed loop control system, it will complement by itself. If these errors are too big, clearly the braking performance will be effected, but if these errors are not so big, what will happen, if our ABS system will deal with these changes or not. So it is necessary to do more work in future based on this factor.

Adaptive Motor Bias Value In the last chapter, we design a frequency splitter and introduce a motor bias value. From sensitivity analysis of this value, we can see if the bias choose too small or too large, during the ABS control cycle, the lower part or the upper part of the motor torque will be saturated, and the braking performance is losing. In this project we already estimated the boundary between the braking distance and the recovered energy these two cost functions, in future still more precisely work should be done.

Finally, more future work could also be done to expand the Quarter Car Model (QCM) into a more advanced model, for instance by introducing wheel coupling or weight shifting of the vehicle.

Appendix A

Simulation schematic

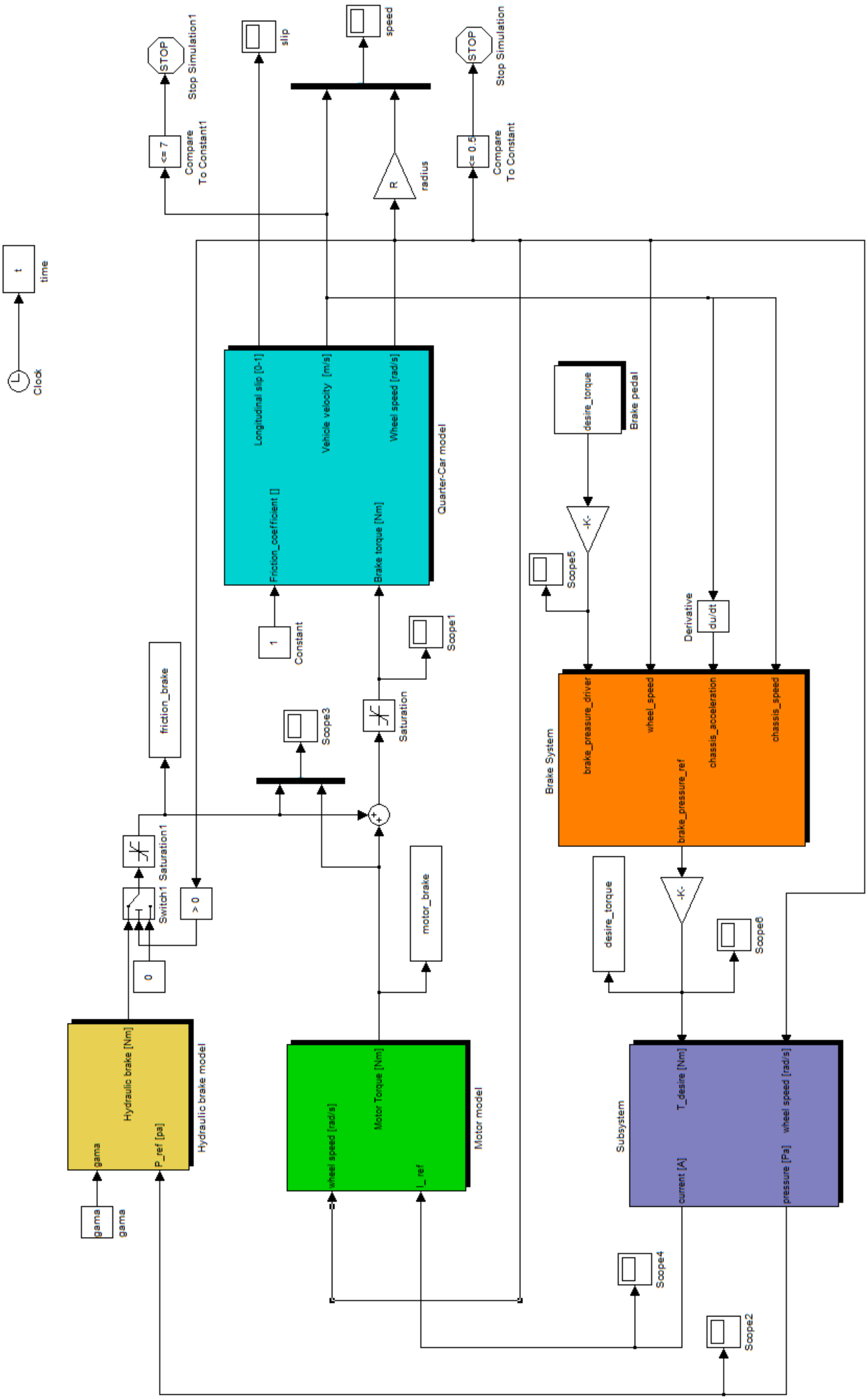

Figure A-1: Final simulation programme

Bibliography

[1] L. Situ, "Electric vehicle development: The past, present and future," in *3rd International Conference on Power Electronics Systems and Applications*, 2009.

[2] *http://www.abiresearch.com/eblasts/archives/analystinsider_template.jsp?id=197*.

[3] *http://auto.howstuffworks.com/auto-parts/brakes/brake-types/regenerative-braking.htm/printable*.

[4] H. Yeo, D. Kim, S. Hwang, and H. Kim, *Regenerative Braking Algorithm for a HEV with CVT Ratio Control During Deceleration*. PhD thesis.

[5] S. R. Cikanek and K. E. Bailey, "Regenerative braking system for a hybrid electric vehicle," in *American Control Conference, Anchorage, AK May 8-10*, 2002.

[6] J. K. AHN, K. H. JUNG, D. H. KIM, H. B. JIN, H. S. KIM, and S. H. HWANG, "Analysis of a regenerative braking system for hybrid electric vehicles using an electro-mechanical brake," *International Journal of Automotive Technology*, vol. 10, pp. 229–234, 2009.

[7] H. B. Pacejka, *Tyre and Vehicle Dynamics*. London: Butterworth-Heinemann, 2006.

[8] U. Kiencke and L. Nielsen, "Automotive control systems: For engine, driveline, and vehicle," *Measurement Science and Technology*, vol. 11, no. 12, p. 1828, 2000.

[9] R. Johansson and A. e. Rantzer, *Nonlinear and Hybrid Systems in Automotive Control*. London: Springer-Verlag, 2003.

[10] S. M. Savaresi, M. Tanelli, and C. Cantoni, "Mixed slip-deceleration control in automotive braking systems," *Journal of Dynamic Systems, Measurement, and Control*, vol. 129, no. 1, pp. 20–31, 2007.

[11] T. A. Johansen, I. Petersen, J. Kalkkuhl, and J. Ludemann, "Gain-scheduled wheel slip control in automotive brake systems," *Control Systems Technology, IEEE Transactions on*, vol. 11, no. 6, pp. 799–811, 2003.

[12] G. Mathieu, P.-L. William, d. V. Edwin, and V. Michel, "Improvements to a five-phase abs algorithm for experimental validation," *Vehicle System Dynamics*, vol. 00, pp. 1–22, 2010.

[13] R. B. GmbH, *Bosch Handbook for Automotive Electrics - Automotive Electronics*. Bentley Publishers, 2007.

[14] J. S. Yu, "A robust adaptive wheel-slip controller for antilock brake system," in *Decision and Control, 1997., Proceedings of the 36th IEEE Conference on*, vol. 3, pp. 2545–2546 vol.3, 1997.

[15] I. Petersen, T. Johansen, J. Kalkkuhl, and LÍźdemann, "Wheel slip control in abs brakes using gain scheduled constrained lqr," 2001.

[16] M. Tanelli, A. Astolfi, and S. M. Savaresi, "Robust nonlinear output feedback control for brake by wire control systems," *Automatica*, vol. 44, no. 4, pp. 1078–1087, 2008.

[17] W. Pasillas-LÍępine, "Hybrid modeling and limit cycle analysis for a class of five-phase anti-lock brake algorithms," *Vehicle System Dynamics: International Journal of Vehicle Mechanics and Mobility*, vol. 44, no. 2, pp. 173–188, 2006.

[18] J. Lygeros, K. H. Johansson, S. N. Simic, Z. Jun, and S. S. Sastry, "Dynamical properties of hybrid automata," *Automatic Control, IEEE Transactions on*, vol. 48, no. 1, pp. 2–17, 2003.

[19] A. Van der Schaft and O. Schumacher, *An Introduction to Hybrid Dynamical Systems*. London: Springer UK, 2008.

[20] L. Chih-Min and C. F. Hsu, "Self-learning fuzzy sliding-mode control for antilock braking systems," *Control Systems Technology, IEEE Transactions on*, vol. 11, no. 2, pp. 273–278, 2003.

[21] D. E. Nelson, R. Challoo, R. A. McLauchlan, and S. I. Omar, "Implementation of fuzzy logic for an antilock braking system," in *Systems, Man, and Cybernetics, 1997. 'Computational Cybernetics and Simulation'., 1997 IEEE International Conference on*, vol. 4, pp. 3680–3685 vol.4, 1997.

[22] W. Wei-Yen, H. Kou-Cheng, L. Tsu-Tian, and C. Guan-Ming, "Robust sliding mode-like fuzzy logic control for anti-lock braking systems with uncertainties and disturbances," in *Machine Learning and Cybernetics, 2003 International Conference on*, vol. 1, pp. 633–638 Vol.1, 2003.

[23] L. Chih-Min and C. F. Hsu, "Neural-network hybrid control for antilock braking systems," *Neural Networks, IEEE Transactions on*, vol. 14, no. 2, pp. 351–359, 2003.

[24] S. Drakunov, U. Ozguner, P. Dix, and B. Ashrafi, "Abs control using optimum search via sliding modes," in *Decision and Control, 1994., Proceedings of the 33rd IEEE Conference on*, vol. 1, pp. 466–471 vol.1, 1994.

[25] W. K. Lennon and K. M. Passino, "Intelligent control for brake systems," *Control Systems Technology, IEEE Transactions on*, vol. 7, no. 2, pp. 188–202, 1999.

[26] P. E. Wellstead and N. B. O. L. Pettit, "Analysis and redesign of an antilock brake system controller," *Control Theory and Applications, IEE Proceedings -*, vol. 144, no. 5, pp. 413–426, 1997.

[27] H. Yeo and H. Kim, "Hardware-in-the-loop simulation of regenerative braking for a hybrid electric vehicle," *Proceedings of the Institution of Mechanical Engineers, Part D: Journal of Automobile Engineering*, vol. 216, no. 11, pp. 855–864, 2002.

Glossary

List of Symbols

Abbreviations

ϵ	ABS threshold (m/s^2)
γ	Brake pad friction coefficient (no dimension)
λ	Wheel slip (no dimension)
μ	Coefficient of friction (no dimension)
ω	Wheel speed (rad/s)
F_c	Cut frequency (Hz)
F_x	Friction force (N)
F_z	Vertical load (N)
J	Wheel inertia $(kg \cdot m^2)$
J_m	Motor inertia $(kg \cdot m^2)$
m	Quarter mass of the vehicle (kg)
R	Tyre radius (m)
T_b	Brake torque (Nm)
T_f	Friction brake torque (Nm)
T_m	Electric motor brake torque (Nm)
u	ABS pressure derivative (Pa)
v	Vehicle speed (m/s)